AD-A050 193 AERONAUTICAL RESEARCH COUNCIL LONDON (ENGLAND) F/G 20/4
THE PERFORMANCE OF A 6.5 PRESSURE RATIO CENTRIFUGAL COMPRESSOR --ETC(U)
1977 M G JONES
UNCLASSIFIED ARC-CP-1385 NL

| OF |
AD
A050193

END
DATE
FILMED
3-78
DDC

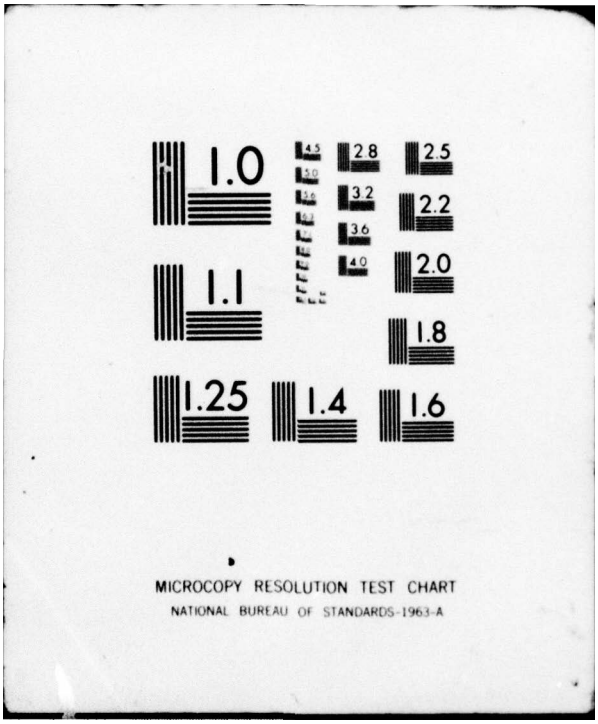
1.0
1.1
1.25
1.4
1.6
1.8
2.0
2.2
2.5
2.8
3.2
3.6
4.0
MICROCOPY RESOLUTION TEST CHART
NATIONAL BUREAU OF STANDARDS-1963-A

C.P. No.1385*
September 1976

THE PERFORMANCE OF A 6.5 PRESSURE RATIO CENTRIFUGAL COMPRESSOR HAVING A RADIALLY-VANED IMPELLER

- by -
M.G. Jones

SUMMARY

The aerodynamic design and experimental performance of a centrifugal compressor designed for a pressure ratio of 6.5 and a specific speed of 68 are described. The compressor consisted of a radially-vaned impeller and a transonic, vaned radial diffuser. At design speed a peak overall total-to-total isentropic efficiency of 0.746 was achieved at the maximum pressure ratio of 5.9, rising to 0.79 at a pressure ratio of 3.5 at 80 per cent speed. A theoretical analysis of the impeller channel flow suggests that high vane-to-vane aerodynamic loading was partly responsible for the shortfall in performance. The impeller was also tested with a vaneless diffuser and a detailed analysis is made of static pressure measurements on the impeller shroud and vaneless and vaned diffuser walls. Several recommendations are made regarding the design and testing of centrifugal compressors.

*Replaces NGTE R 342 - ARC.37 043.

CONTENTS

1.0 Introduction

The requirement in the past decade or so for small gas turbine engines for advanced helicopter propulsion and for other aeronautical applications such as auxiliary power units has renewed interest in the centrifugal compressor which gave way to the axial machine for larger aircraft powerplants during the 'fifties. The centrifugal's advantages of simplicity, ruggedness, stability of operation and possible greater efficiency at high pressure ratios in small sizes are now widely recognised. A programme of centrifugal compressor research was therefore initiated at the National Gas Turbine Establishment (NGTE) in 1971.

It can be shown by means of simple cycle calculations with a turbine entry temperature consistent with uncooled blades, an important factor in reducing cost and complexity in small engines, and assuming best current component efficiencies, that minimum specific fuel consumption is obtained at an overall cycle pressure ratio of at least 8. At the present time, the highest overall compression efficiency for such pressure ratios would be obtained not from a single centrifugal compressor stage but from a combination of a centrifugal stage preceded by one or more axial stages, in which case the greater the proportion of the compression done by the axial stages the higher the optimum overall pressure ratio. A common arrangement, being a convenient compromise between complexity and efficiency, is to use a single axial stage ahead of a centrifugal, in which case the cycle calculations give an optimum overall pressure ratio of about 9. Assuming a pressure ratio from the axial stage of around 1.4, that for the centrifugal becomes about 6.5.

The other major parameter defining the duty of a centrifugal compressor is specific speed which is a function of impeller rotational speed, mass flow and work input. At least two slightly different formulae for specific speed exist and the one which will be used in this Report is due to Balje[1]. Various attempts have been made to correlate centrifugal compressor efficiency with specific speed and to define an optimum value for the latter. However, examination of a number of engine designs shows that, for a given pressure ratio, the specific speed of the centrifugal compressor is limited by turbine blade stressing considerations to a value below any such aerodynamic optimum. This limiting specific speed is lower for a centrifugal compressor forming part of an axial-centrifugal compressor combination than for one which provides the whole compression of the cycle.

This Report describes the aerodynamic design and experimental performance evaluation of a centrifugal compressor having an overall pressure ratio of 6.5 and a specific speed of 68, these values rendering the design relevant to an axial-centrifugal compressor system. Referred to as compressor C139A, the design used a single-sided aluminium alloy impeller with radially-stacked vanes and a transonic vaned radial diffuser.

2.0 Compressor design

The design duty for the compressor was as follows:

Overall pressure ratio	6.5
Overall isentropic efficiency	0.8
Mass flow	1.814 kg/s
Rotational speed	40,000 rev/min
Specific speed	68

A list of all the main design parameters is given in Table I and the layout of the compressor is shown diagrammatically in Figure 1.

2.1 Impeller

Initially, a one-dimensional flow analysis was used to provide the overall dimensions of the impeller such as tip diameter. Based on this data an empirical geometrical specification was laid down for the complete impeller. The hub and shroud wall contours were made up of circular arcs and the necessary twist and form were given to the vanes by specifying a camber line at the inlet shroud radius and prescribing that the vanes were stacked radially. The form of the camber line was relatively simple in that it was straight for the leading edge region of the vane, followed by a circular arc and finally became straight and parallel to the axis of rotation approximately halfway through the impeller flow path. The circumferential thickness of the vanes was specified by simple straight line contours in the meridional plane. Intervanes, having the same camber line and thickness as the main vanes, were also included in the radial portion of the impeller.

Having formulated a complete and detailed geometrical specification for the impeller, it was decided to take the design a stage further and assess the internal aerodynamics using the Matrix Throughflow technique[2] in which the flow in a meridional stream surface is analysed. For this design exercise the shape of the mean stream surface was taken to be that of the vane camber surface. This implies no allowance for slip or deviation at the impeller tip but it was considered that this assumption would not detract from the value of using the throughflow analysis as an aid in selecting an impeller design. To allow for the flow blockage due to the presence of the

vanes, the thickness of the stream surface was taken to be proportional to the ratio of vane thickness to vane pitch. The most difficult problem in applying throughflow analysis is the modelling of the flow losses and allowance for blockage created by the annulus wall boundary layers. For the present task a simple approach was adopted of taking account of viscous effects by assuming a constant local polytropic efficiency throughout the flow field with no allowance for boundary layer blockage.

The throughflow analysis provides the distribution of relative velocity along the hub and shroud. These velocities represent some mean of the relative velocities on the vane suction and pressure surfaces and so provide a measure of the rate of diffusion and boundary layer growth along the vane surfaces for assessing the impeller design. To provide a means for judging the design of blade profiles for axial turbomachines, Smith[3] examined a simple flow model in which the free stream velocity decreased linearly with distance along the profile boundary. By applying two-dimensional boundary layer theory Smith concluded that, to avoid flow separation, the velocity ratio should not exceed 1.5. Dallenbach[4] came to a similar conclusion in a centrifugal compressor study. Whilst it was appreciated that the flow within a centrifugal compressor is highly three-dimensional, it was decided, in the absence of more relevant information, to assess the velocity distributions for the current impeller design using the simple flow model of Dallenbach and Smith.

The result of applying throughflow analysis to the initial empirical specification for the impeller was to show that the geometry was unacceptable in that the relative velocity ratio for the shroud of 3.5 was far in excess of the limiting value of about 1.5. Following this analysis four modifications to the impeller geometry were made before reaching the final design specification. The value of the throughflow analysis can be seen in Figure 2 which compares the hub and shroud wall velocities for the initial and final impeller geometries. The final design is considered to be superior on two accounts. Firstly, the adverse velocity gradient for the shroud is much reduced and, secondly, there is a smaller difference between the hub and shroud velocities in the region of the impeller outlet. These two factors should provide improved flow conditions within the impeller and at entry to the diffuser.

The final geometrical specification for the impeller is given in Figures 3 and 4 and Table I. The method of defining the geometry is very similar to that described above for the initial design except that the final

shroud wall contour is defined by a "supercircle" or Lamé oval. The vane camber surface is defined in Figure 4 in terms of a camber line for which the radial stacking criterion has allowed the circumferential co-ordinate to be non-dimensionalised according to radius.

2.2 Diffuser

A vaned radial diffuser having a straight channel centre-line was designed on the principle of a short vaneless space between the impeller tip and diffuser vane leading edge with a transonic approach Mach number. The radius at the vane leading edge was therefore chosen as 5 per cent greater than impeller tip radius and the radius at the vane trailing edge was selected as being representative of the limiting value which would be imposed in an actual engine application by considerations of frontal area and weight. Parallel front and rear walls separated by an axial distance equal to the tip width of the impeller were employed. The diffusion was achieved by giving the side walls of each channel a "trumpet" shape with an included angle of only 1^{o} at the throat increasing towards the channel outlet. Based on an estimate of the flow conditions at diffuser approach, zero incidence was specified with the suction surface of the vanes.

Taking account of the required throat area and of the desirability of a throat channel aspect ratio in the region of unity, the number of vanes and the channel outlet included angle were selected to give suitable values of channel length/throat width and area ratio. These were chosen by reference to the appropriate diffuser performance map presented by Runstadler[5], the chosen operating point being determined by considerations of maximum static pressure recovery coefficient consistent with remaining within the assumed region of "no appreciable stall" defined in Figure 3 of that reference.

The initial diffuser design was designated A1. A single channel is shown in Figure 5 and the main design parameters are given in Table I.

3.0 Compressor experimental test facility

3.1 Test rig

A schematic layout of the test rig is given in Figure 6. The compressor was driven by an air turbine through a 2/1 step-up gearbox. The impeller was "overhung", being bolted to the drive shaft by means of a flange on the back face. The drive shaft ran in two preloaded, squeeze-filmed, angular-contact ball bearings and also carried a balance piston to remove most of the aerodynamic axial thrust load. Air entered the compressor from atmosphere and passed axially through a flow-measuring venturi nozzle into a

plenum chamber from which the convergent inlet duct led into the impeller eye. After leaving the compressor, the flow entered a scroll-type collector having a single tangential outlet connected, by a short divergent duct, to a throttle valve. Downstream of the valve, the flow was further diffused and turned by a 90^{o} cascade elbow into a flow-straightening section followed by an orifice plate flowmeter. After further expansion and another turn through 90^{o}, the flow joined the turbine exhaust stream.

3.2 Instrumentation

The compressor and test rig were fitted with comprehensive instrumentation to permit a detailed evaluation of the aerodynamic performance of the impeller and diffuser. In addition, instrumentation for monitoring the mechanical integrity of the compressor was incorporated.

3.2.1 Aerodynamic instrumentation

Before describing the aerodynamic instrumentation it is necessary to explain that, in addition to the measurement of the overall stage performance of the impeller and vaned diffuser, the performance of the impeller alone was investigated by running it in conjunction with a vaneless diffuser.

Static pressure tappings were situated in the plenum chamber, in the impeller inlet and shroud casing, on the front and rear walls of the vaneless and vaned diffusers and in the outlet duct. Figure 7 shows the locations of tappings in the inlet and shroud casing. Within the limitations imposed by space and other instrumentation, the main objective was to have fairly complete sets of tappings in two circumferential positions (radial planes B and D). Figure 8 shows the location of tappings in the vaneless diffuser where, basically, eight radial planes with tappings at various radii repeated on both walls were used. Figure 9 shows the arrangement of tappings in a vaned diffuser. Two, approximately diametrically opposite, channels were selected to have a complete set of centre-line tappings and eight others to have tappings at channel throat and exit only. Since the front wall of the vaned diffuser was the same as that of the vaneless diffuser, only those tappings occurring in the vaneless space were used on that wall. All pressures were measured on mercury or water manometers.

Air temperature was measured using stagnation, half-shield type chromel-constantan thermocouples at entry to the compressor (in the plenum chamber), at diffuser exit and in the collector outlet duct. At each of these three stations four thermocouples were used.

Rotational speed was set by means of an "$N/\sqrt{T}$ meter". This is a stroboscopic device in which a marked rotating disc, driven through a tachometer from the turbine shaft, is viewed under a light whose frequency can be adjusted by a calibrated capacitor to allow for variation of compressor inlet temperature. The actual compressor rotational speed was measured by means of a magnetic pick-up sensing the passing frequency of a toothed wheel incorporated in the gearbox-to-compressor connecting shaft and was displayed on a Venner digital counter.

Air mass flow was measured by a venturi nozzle to BS 1042 specification located upstream of the plenum chamber, as shown in Figure 6, static pressures being measured by four tappings at inlet and eight tappings at the throat. A back-up and cross-check for this instrument was provided by an orifice plate, also to BS 1042, situated in the outlet duct (see Figure 6), static pressures being measured by four tappings one diameter upstream and four half a diameter downstream and temperature by a single upstream thermocouple.

3.2.2 Mechanical instrumentation

In order to continuously monitor possible vibrational stresses in the impeller vanes a total of eight strain gauges were attached to the inducers of two, approximately diametrically opposite, vanes, the inducer being considered to be the region likely to experience the highest such stresses. The signals from the strain gauges were fed, via a slip ring unit enclosed in the intake bullet (Figure 1), to an ultra-violet galvanometer recorder.

A continuous check on the vibration levels of the rig was kept by means of accelerometers mounted in pairs with perpendicular axes on the intake flange just upstream of the impeller leading edge, on the rear of the impeller casing and on the turbine casing. Velocities greater than 2 to 3 cm/s were considered to be excessive. A check on orbital motion of the impeller was provided by two inductive displacement transducers on perpendicular axes reading from the slip ring drive extension upstream of the impeller hub. The maximum allowable radius of orbit was 50 to 75 μm.

Several devices were incorporated in the rig to measure and maintain impeller vane shroud clearance. Cut wire probes were situated in a number of positions in the impeller shroud casing. These incorporate a loop of copper wire projecting from the casing surface by a distance equal to the required minimum clearance so that, if the clearance during test becomes too small, the wire is cut through thus breaking an electrical circuit and causing the air supply to the driving turbine to be shut off. Actual minimum clearance

occurring during each test was recorded by soft metal plugs projecting from the casing which were removed after running and the amount by which the impeller vane tips had cut them back measured. At each test speed, readings of the vane clearance were taken whilst running using two Fenlow probes at the same radial position on the casing (about 6 per cent less than impeller tip radius) but separated circumferentially by 90^{o}. These enable the clearance of a moving rotor to be determined by measuring the amount by which a moving probe has to be driven towards the rotor before reaching the known clearance at which a capacitor connected to the probe discharges.

4.0 Overall performance

Seven builds of the compressor were tested, as summarised in Table II. For most builds, tests were conducted at a range of speeds up to the design speed of 40,000 rev/min. The performance parameters quoted in the following sections have, where appropriate, been corrected to the standard inlet conditions of 101.32 kN/m^2 pressure and 288.15 K temperature. Definitions of the parameters are given in Appendix A.

4.1 Builds I and II - Design impeller with vaneless diffuser

These builds of the design impeller with a vaneless diffuser were devoted to mechanical and instrumentation checks, notably adjustment of the impeller shroud clearance to prevent contact between the vane tips and shroud casing at the higher speeds.

It is desirable for the clearance at design speed to be as small as is practicable to reduce losses due to flow recirculation. Some allowance has to be made, however, for possible temporary reduction in clearance at the surge condition due to the extra loads imposed on the compressor components and a minimum design point running clearance of about 400 μm was considered appropriate for the present compressor. Accordingly, for the first build, the shroud casing inner contour was designed to give a static clearance on assembly of approximately 400 μm along the whole length of the impeller shroud. Upon running the impeller (Build I) it was found that the clearance near the impeller tip was reducing with increasing rotational speed due, probably, to "dishing" of the impeller under centrifugal loading. For Build II the static clearance in this region was therefore increased by 150 μm by shimming the whole of the diffuser, collector, shroud casing and intake assembly axially upstream relative to the impeller drive shaft casing. This static clearance still proved, however, to be insufficient to allow the design speed to be reached whilst retaining the required running clearance and it was not until Build III, described below, that this situation was achieved.

4.2 Build III - Design impeller with vaneless diffuser

This build of the compressor was the first associated with performance measurement and was concerned with an evaluation of the flow characteristics of the impeller only. For this purpose the compressor build consisted of the design impeller with the vaneless diffuser. Based on the outcome of Builds I and II, the impeller shroud static clearance was increased by a further 100 μm axially resulting in the required running clearance at design speed of approximately 400 μm near the impeller tip.

Figure 10 shows the impeller performance characteristic based on static pressure measurements taken at a radius of 133.35 mm in the vaneless diffuser rather than at the actual impeller tip radius of 124.46 mm. The reasons for this choice of station will be given in a later Section. The temperature used to calculate the impeller efficiency was that at diffuser exit. Table III gives the values of a number of parameters derived from the test measurements at the nearest test point to the maximum pressure ratio for each speed.

It can be seen that the maximum flow at the design speed was about 7 per cent below the design flow of 1.814 kg/s. This was thought to be due to choking in the inducer throat. It should be noted, however, that, at the lower speeds, where the flow characteristic does not become vertical, the maximum flow is determined by choking of the throttle valve. Flow range is therefore not given in Table III for these speeds. This also applies to the results of a later vaneless diffuser build.

4.3 Build IV - Design compressor stage

Whilst the vaneless diffuser build described above showed the flow capacity of the design impeller to be below the design target, it was considered desirable to evaluate the stage performance of the compressor consisting of the design impeller and the A1 vaned diffuser. It was found that the maximum flow at design speed was further reduced by approximately 6 per cent indicating choking in the diffuser.

4.4 Build V - Modified impeller with vaneless diffuser

At this point in the experimental programme it was clear from the performance characteristics of the impeller alone, Build III, and of the complete stage, Build IV, that it was necessary to modify the design compressor stage in order to pass the design mass flow. Considering the impeller first, the leading edges of the vanes were cut back axially by 5.08 mm in order to increase the throat area, as indicated in Figure 11, and hence the choking mass flow. The impeller, thus modified, was then tested with the vaneless diffuser as used in Build III.

The full lines in Figure 12 show the resulting impeller performance characteristic for the same station of 133.35 mm radius used in deriving the characteristic for the design impeller Build III, Figure 10, and Table IV gives the values of other salient parameters. The success of the modification to the impeller can be seen from Figure 12 which shows that the maximum mass flow at design speed was significantly increased and exceeded the design target.

4.5 Build VI - Modified compressor stage

Having achieved an acceptable maximum mass flow for the modified impeller the next step in the programme was to modify the vaned diffuser in order that the complete stage should pass the design mass flow. This in fact necessitated the design of an entirely new vaned diffuser, designated A2, having increased throat area compared to A1. The design philosophy for this diffuser was identical to that described in Section 2.2 for the original design but, owing to the requirement to use the same collector, the overall diameter of the A2 diffuser had to remain the same as for A1, resulting in reduced channel length/throat width and area ratio and, hence, a slightly lower pressure recovery as predicted by Reference 5.

Figure 13 shows the overall performance characteristic for the compressor stage, consisting of the modified impeller and A2 diffuser, based on diffuser exit total pressure calculated from measured static pressure and channel exit geometrical area. Table V gives the values of other parameters. The characteristic showed that the maximum flow at design speed was about 4 per cent less than for the vaneless diffuser build (Figure 12), implying that, although the A2 diffuser was passing about 12 per cent more flow than A1, the increase in diffuser throat area had not been quite sufficient. The most notable feature of the characteristic, however, was the considerably reduced flow range at each speed compared to the vaneless diffuser build, although some reduction in range was to be expected due to the change to a vaned diffuser. Efforts to understand this led to an analysis of the static pressure measurements at exit from the vaned diffuser which revealed a circumferential variation amounting to over twice the average dynamic head, as shown in Figure 14. Individual diffuser channels would, therefore, pass widely differing mass flows and it was presumed that those passing the lower flows were causing premature surge thus restricting the compressor flow range. It was concluded that the scroll-type collector was causing the non-uniformity of static pressure at diffuser exit, either by its close proximity to the diffuser vanes or because its cross-sectional area was not

correctly matched to the inlet flow conditions at all circumferential positions. It may be seen from Figure 14 that the sudden rise in static pressure occurred in the region of the collector scroll tongue position, suggesting that incorrect matching was the more likely cause.

4.6 Build VII - Modified compressor stage with redesigned collector

The final build of the compressor incorporated the modified impeller and A2 vaned diffuser with the flow discharging into a redesigned scroll-type collector intended to eliminate the non-uniformity of flow at diffuser exit experienced in Build VI. The new collector featured two major changes from the original design. Firstly, the radial distance between the diffuser vane trailing edges and the scroll entry was increased from approximately 12 mm to 59 mm. Secondly, the scroll cross-sectional area was more than doubled everywhere so that, whilst tangential velocity within it was still designed to remain constant circumferentially, no attempt was made to preserve the inlet dynamic head by area matching. The design scroll exit Mach number was approximately 0.1. Although the inefficiency caused by such rapid dumping of dynamic head would be undesirable in an actual engine application, it was unimportant in the case of this research compressor whose overall performance was measured upstream of the collector.

The compressor build incorporated additional instrumentation in the form of eighteen Kiel total pressure probes positioned just downstream of the diffuser vane trailing edges in six circumferentially equispaced axial rakes of three each. The object was to give more reliable total pressure measurements, for the purposes of obtaining the overall performance characteristic, than those derived for previous builds from static pressure measurements and the characteristic based on the Kiel probe readings is shown in Figure 15. In fact, for this build, it was found that the characteristic derived from static pressures was in very close agreement with that presented, thus vindicating the use of this method in earlier builds. Total-to-static efficiencies are also shown on the characteristic as these are often used in published work by other organisations since they represent the most pessimistic assumption regarding diffusion subsequent to the vaned diffuser, that all the dynamic head is lost, whereas the total-to-total efficiency assumes complete pressure recovery. Study of a number of actual engine applications of centrifugal compressors shows that, in practice, between 75 and 90 per cent of the dynamic head is recovered. Comparing Figures 13 and 15, a considerable increase in flow range is evident as a result of the

redesigned collector giving a uniform static pressure at diffuser exit as shown in Figure 14.

The maximum overall pressure ratio and total-to-total isentropic efficiency at design speed fell considerably short of the design values of 6.5 and 0.8 respectively. The work input parameter was very close to its design value, however, so that the shortfall in pressure ratio corresponded to that in efficiency. In retrospect, the design efficiency may be considered to have been unrealistically high in view of the non-optimisation of specific speed referred to in the Introduction. It can be estimated from the correlation of Reference 6 that this might result in an efficiency drop of 2 to 3 points. By the time that the testing of the compressor had been completed, the throughflow analysis method had been further developed, enabling an estimation of vane-to-vane aerodynamic loading in the impeller to be made. The result is shown in Figure 16, the loading parameter being defined as:

$$\frac{\Delta p}{\gamma p M^2}$$

where Δp is the static pressure difference from vane to vane across an impeller passage,

γ is the ratio of specific heats,

p is the mean stream surface static pressure, and

M is the mean stream surface relative Mach number.

The sudden drop in loading at about 40 per cent meridional distance on each surface is due to the start of the intervanes. Reference 7 suggests the limiting value of loading parameter for avoidance of suction surface boundary layer separation to be about 0.7 and this was clearly exceeded at the shroud. It seems likely that this high loading was largely responsible for the remaining 2 to 3 points difference in efficiency between the design value of 0.8 and the measured 0.746.

4.7 Choice of impeller exit station

It is widely accepted that the unmixed flow at the exit from a centrifugal impeller is complex and that a total pressure leading to a meaningful impeller efficiency cannot be derived from the static pressures indicated by conventional tappings located at the tip of the impeller. Of more potential use is a static pressure measurement sufficiently far downstream that the flow can be considered to have mixed out. The problem then, however, in deriving the total pressure from such a static pressure measurement, is in what assumptions to make concerning, firstly, blockage due to wall boundary

layers and, secondly, flow direction. In analysing the results of the impeller tests described in this Report the very simple assumptions of zero blockage and free vortex flow from the impeller tip to the required station were made. The characteristics for the modified impeller (Build V) derived on this basis at 133.35 mm radius and that based on static pressure measurements at the actual impeller tip radius of 124.46 mm are shown in Figure 12 and Table VII compares the efficiencies at a common flow at design speed. Also given in the table is the overall or compressor stage efficiency, for the same conditions of flow and speed, for the final Build VII. The selected test point was also simulated using a loss-modelling compressor performance prediction program in which it is assumed that mixing-out occurs, in effect, instantaneously at the impeller tip. The difference between the efficiency after mixing and that at vaned diffuser exit predicted by the program is also given in Table VII. Comparison of the test and predicted figures shows a much greater difference between the impeller tip and overall efficiencies for the test results (0.100 compared to 0.055). In fact, the predicted difference is much more closely equated by the test efficiency difference of 0.051, from 133.35 mm radius to diffuser exit. It is reasonable to take the overall efficiency as a common datum since the test total pressures at the diffuser exit station are thought to be reliable, the same values having been obtained by two independent methods (see Section 4.6). On this basis it would appear that the test impeller efficiency at 133.35 mm radius is close to the predicted impeller "mixed-out" efficiency. Whilst avoiding the placing of too much reliance on the prediction program, there does, therefore, appear to be justification for presenting the impeller characteristics on the basis of measurements at 133.35 mm radius.

5.0 Detailed static pressure measurements

5.1 Impeller shroud

At the design speed of 40,000 rev/min measurements were made of the static pressure distribution on the impeller shroud at two mass flows. The results are shown for the modified impeller tested with the vaneless diffuser (Build V) and with the A2 vaned diffuser and redesigned collector (Build VII) in Figures 17 and 18 respectively. It will be seen that the results for the vaned diffuser build exhibit greater scatter near the impeller tip than is the case with the vaneless diffuser. This is in accordance with the analysis by Dean et al[8] of the experimental results of Welliver and Acurio[9] which showed similar scatter, attributed to the extension of the vaned diffuser pressure field upstream into the impeller channels.

Shown superimposed on the experimental results are theoretical predictions from the Marsh throughflow program[2] using local values of polytropic efficiency in the impeller estimated from the experimental results. Agreement is generally quite good, especially for the vaned diffuser Build VII, but the theory tends to underestimate the static pressure near the tip. The comparison in this region may be confused by several factors. Firstly, the assumed value of polytropic efficiency may be locally incorrect. Secondly, the existence of a region of separated flow near the impeller tip, as has been demonstrated experimentally by a number of workers (listed in Reference 10), would probably result in a time-averaged pressure somewhat different from the prediction which is for a mean stream surface based on full channel flow. Thirdly, it is shown in Reference 11 that the indicated reading of a conventional static pressure tapping can be significantly different from the true time-average of a fluctuating pressure.

The flow model hypothesised by Dean[8] consists of an isentropic throughflow jet, initially filling the impeller passage and then separating from the blade suction surface, leaving a stationary wake. The overall impeller loss is realised when the jet and wake mix downstream of the impeller tip. In an attempt to check the validity of this model, several throughflow calculations were made for the vaneless diffuser Build V with a local polytropic efficiency of unity within the impeller and with the wake region simulated by additional vane thickness starting at about 75 per cent meridional distance. Figure 19 shows the results of this analysis. Whilst it is difficult to draw any real conclusions regarding the separated region, since the extent of the wake is unknown, the analysis does show that, in the assumed pre-separation zone, the assumption of isentropic flow is inappropriate.

5.2 Vaneless diffuser

For Build V, consisting of the modified impeller and vaneless diffuser, detailed measurements were made of the static pressure on the vaneless diffuser walls at two points on the design speed characteristic, the pressure tappings being disposed at various combinations of radial and circumferential position as shown in Figure 8. The radial distribution of static pressure obtained is shown in Figure 20, where each test result value is simply the mean of the several readings, on both walls, for that radius. Also shown are the theoretical results of the performance prediction program referred to in Section 4.7 starting from impeller tip conditions derived from the measured

static pressure at the impeller tip radius of 124.46 mm. Although Section 4.7 would suggest that the conditions at 133.35 mm radius would be more appropriate, the way in which the prediction program calculates losses necessitates starting at the actual impeller tip. Whilst there is broad agreement between test results and theory, the former exhibit considerable scatter amongst themselves and this prompted a closer examination of the individual readings. Figure 21 shows these plotted against circumferential position for the two radial locations at which there were more than two tappings on either wall. It may be seen that the pressures on the two walls are in close agreement, enabling a mean circumferential distribution to be justifiably plotted. There is, however, a marked circumferential variation of pressure which follows a very similar pattern for both mass flows and for both radii except that the trough at about 270° is less pronounced at the larger radius. This vaneless diffuser build used the original design of collector which, when employed in the vaned diffuser Build VI, caused the variation of static pressure at diffuser exit described in Section 4.5 and shown in Figure 14. Although the shape of the pressure distribution in Figure 21 is somewhat different to that for Build VI in Figure 14, it is felt that the cause of the distortion was probably the same. For comparison, the position of the collector tongue is at about 13° on the axis of Figure 21. A very similar stationary distortion phenomenon in a vaneless diffuser was observed by Eckardt[12] and attributed to the collector. As in the present case, the distortion tended to decrease with increasing radius in the diffuser although the reason for this is not clear.

Because of this circumferential pressure variation, it is clearly meaningless to take a simple average of the readings from all tappings at a given radius, irrespective of their circumferential positions. An area-weighted mean pressure is probably more significant and this can be calculated for the two radii shown in Figure 21 but not directly for other radii where there are, at most, only two circumferential stations. However, for every radial station above 133.35 mm, readings are available for a common angle, as specified in Figure 21, of 135°. Furthermore, because of the similarity in shape of the circumferential distributions, the ratio of area-weighted mean pressure to that at 135° does not change very much between the 133.35 mm and 152.40 mm radial stations. It has therefore been assumed that this ratio varies linearly with radius and, since it is known at two radii, can be calculated for all others. Hence the area-weighted mean static pressure at

each radius has been derived and is shown in Figure 22. Apart from the points at the largest radius, each set of results lies on a smooth curve. If, for each mass flow, this curve is extrapolated to the impeller tip radius of 124.46 mm, impeller pressure ratio and efficiency can be derived from the resulting value of static pressure. These are, for a mass flow of 1.499 kg/s, an impeller pressure ratio of 6.84 and an efficiency of 0.819 and, for a mass flow of 1.731 kg/s, a pressure ratio of 6.37 and an efficiency of 0.788. Reference to Figure 12 shows that these values lie almost exactly on the design speed characteristic based on the 133.35 mm radius results which has already been chosen as representative of true impeller tip conditions (Section 4.7), thus further justifying this choice.

Using these impeller tip conditions as a starting point, the performance prediction program has again been used to estimate the static pressures throughout the vaneless diffuser and the results are shown as the lines labelled "viscid" on Figure 22. These can be seen to diverge from the experimental points with increasing radius, particularly at the higher flow. The assumptions made in the program regarding boundary layer growth therefore appeared to be pessimistic and so, moving to the opposite extreme, an inviscid calculation was performed. Even this, however, gave static pressures below the experimental values. It would seem, therefore, that the area-weighted mean of the measured pressures cannot be validly compared with theoretical predictions. This may be due to insufficiently detailed knowledge of the circumferential pressure variation or to the existence of an axial variation which was not evident from measurements at the walls. Possibly some other type of mean, such as mass flow-weighted would be more valid, but the similarity of the circumferential pressure distributions at different radii suggests that this would merely result in a vertical movement of the experimental curves in Figure 22 and not a change in gradient as required.

5.3 Vaned diffuser

For the redesigned vaned diffuser, A2, sets of static pressure tappings were positioned on the centre-lines of two approximately diametrically opposite channels as shown in Figure 9. The measurements obtained from these tappings at two points on the design speed characteristic for the final Build VII of the compressor are shown in Figure 23. Agreement between the two channels is good and readings from eight other channels at the throat and 62.5 mm downstream stations also agree closely but are omitted from Figure 23 for the sake of clarity.

The performance prediction program already used in the vaneless diffuser analysis will cater for a vaned diffuser, using the data of Reference 5 to estimate the pressure recovery coefficient. In order to obtain starting conditions for the calculation at the impeller tip, it has been assumed that the impeller characteristic based on 133.35 mm radius for Build V (Figure 12) still applies in the presence of a vaned diffuser. The resulting predictions for static pressure at the diffuser vane leading edge, throat and trailing edge stations are shown in Figure 23. At the trailing edge, the experimental and theoretical pressures agree well. Throat pressure is also predicted fairly accurately for the higher mass flow case. At the vane leading edge position, the flow is passing through a shock system in the semi-vaneless space and rapid changes of pressure are occurring in two dimensions. The rather greater scatter of experimental results and discrepancy compared to predicted results in this region is therefore not unexpected.

6.0 Conclusions

The aerodynamic design and experimental evaluation of a centrifugal compressor consisting of a radially-vaned impeller and a transonic, vaned diffuser have been described. The test performance has highlighted shortcomings in the design process, in that the design performance was not achieved, and in the experimental measurement techniques. Accordingly, a number of recommendations can be made regarding the design and testing of centrifugal compressors.

(i) The vane-to-vane aerodynamic loading, $\Delta p/\gamma p M^2$, should be kept as uniform as possible through the impeller. As a guide to the level of loading to be aimed for, the maximum value of about 0.7 suggested by Reference 7 is considered to be useful. With the NGTE design method, these requirements would be satisfied by a rigorous application of the throughflow analysis[2] for which the impeller geometrical specification and data preparation are now computer-based, enabling much quicker convergence on a suitable design.

(ii) When the flow from the diffuser discharges into a collector, this must be of large enough cross-section to avoid non-uniformity of flow at exit from the diffuser causing premature compressor surge.

(iii) Static pressures should be measured at many stations in the impeller tip/vaneless space region to give a basis for developing an improved understanding of the complex flow in this part of the compressor.

(iv) Conventional static pressure tappings in regions where there is likely to be a variation of pressure with time, such as the impeller tip, should be replaced by special tappings giving a true time-averaged reading, of which several types are suggested in Reference 11. These may need to be complemented by dynamic pressure measuring instrumentation at selected stations to indicate the actual form of the time variation.

The design recommendations have been followed in the design of a second compressor having the same duty as the one described in this Report but with impeller vanes swept back at the tip with the aim of achieving significantly better efficiency and flow range.

APPENDIX A

Definitions of performance parameters

Corrected speed

$$= \text{Measured speed} \times \sqrt{\frac{288.15}{\text{measured inlet temperature in K}}}$$

Corrected mass flow

$$= \text{Measured mass flow} \times \frac{101.32}{\text{measured inlet total pressure in kN/m}^2} \times \sqrt{\frac{\text{measured inlet temperature in K}}{288.15}}$$

Impeller pressure ratio

$$= \frac{\text{Total pressure (derived from measured static) at 133.35 mm radius in vaneless diffuser (see Section 4.7)}}{\text{inlet total pressure}}$$

Overall pressure ratio

$$= \frac{\text{Total pressure (derived from measured static or measured directly) at diffuser exit}}{\text{inlet total pressure}}$$

Total-to-total isentropic efficiency

$$= \frac{\text{Inlet temperature} \times \left\{ \left(\frac{\text{outlet total pressure}}{\text{inlet total pressure}} \right)^{\frac{\gamma-1}{\gamma}} - 1 \right\}}{\text{measured temperature rise}}$$

Total-to-static isentropic efficiency

$$= \frac{\text{Inlet temperature} \times \left\{ \left(\frac{\text{outlet static pressure}}{\text{inlet total pressure}} \right)^{\frac{\gamma-1}{\gamma}} - 1 \right\}}{\text{measured temperature rise}}$$

Work input parameter

$$= \frac{\text{Work input to impeller based on temperature rise}}{(\text{impeller tip blade speed})^2}$$

Diffuser total pressure ratio

$$= \frac{\text{Total pressure (derived from measured static or measured directly) at diffuser exit}}{\text{total pressure (derived from measured static) at impeller tip}}$$

Diffuser static pressure recovery coefficient

$$= \frac{\text{Diffuser exit static pressure - throat static pressure}}{\text{throat total pressure - throat static pressure}}$$

Flow range

$$= \frac{\text{Choking flow - surge flow}}{\text{choking flow}}$$

APPENDIX B

Derivation of Mach numbers

The derivations of the relative Mach number at the eye shroud and the absolute Mach numbers at impeller tip and diffuser exit for which values are given in Tables III to VI are shown in this Appendix in the form of flow charts. The symbols used will first be defined:

A	flow area
D	diameter
M	Mach number
N	rotational speed
P	pressure
Q	mass flow
T	temperature
ΔT	temperature rise
U	vane circumferential velocity
V	air velocity
ρ	density

Subscripts

abs	absolute
ax	axial
r	radial
rel	relative
s	static
t	total
w	whirl

The remaining subscripts should be self-explanatory.

Eye shroud relative Mach number

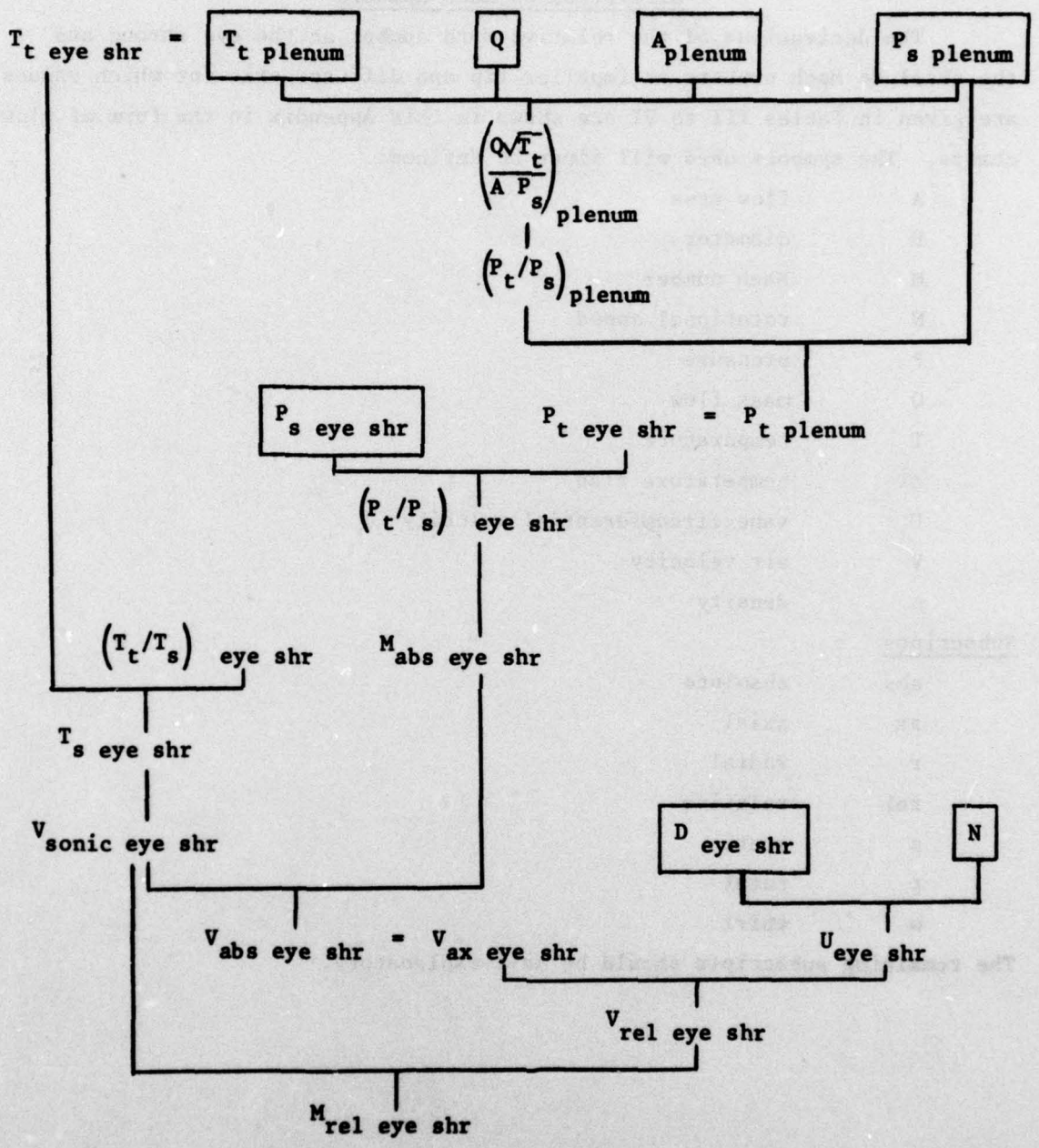

Impeller tip absolute Mach number

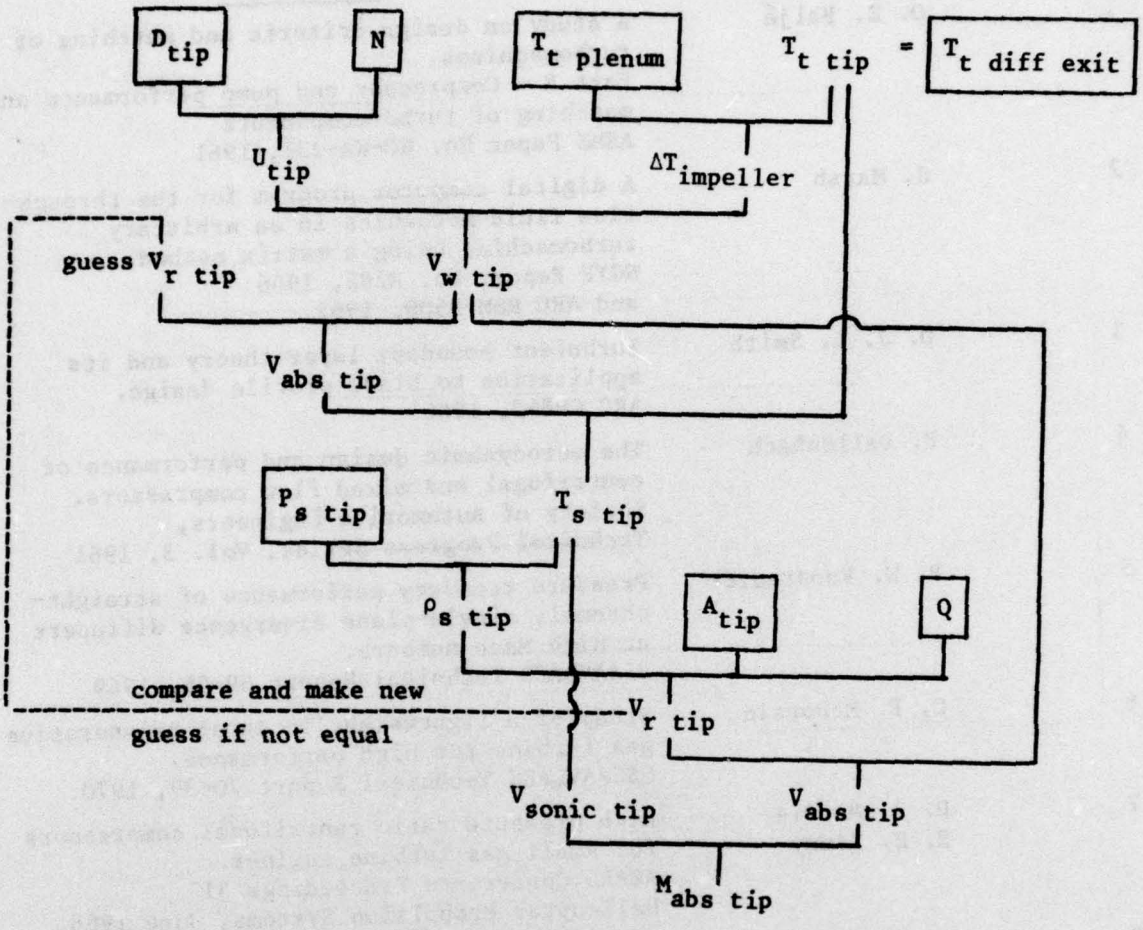

Diffuser exit absolute Mach number

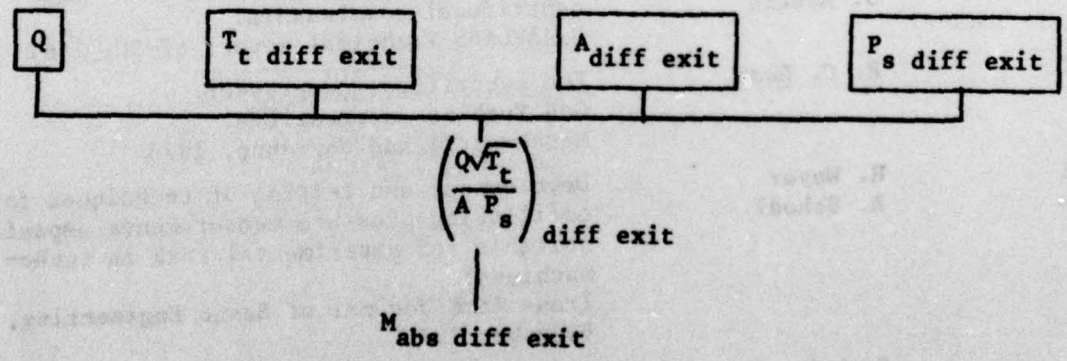

REFERENCES

No.	Author(s)	Title, etc.
1	O. E. Baljé	A study on design criteria and matching of turbomachines. Part B - Compressor and pump performance and matching of turbo-components ASME Paper No. 60-WA-231, 1961
2	H. Marsh	A digital computer program for the through-flow fluid mechanics in an arbitrary turbomachine using a matrix method. NGTE Report No. R282, 1966 and ARC R&M 3509, 1967
3	D. J. L. Smith	Turbulent boundary layer theory and its application to blade profile design. ARC CP868, 1966
4	F. Dallenbach	The aerodynamic design and performance of centrifugal and mixed flow compressors. Society of Automotive Engineers, Technical Progress Series, Vol. 3, 1961
5	P. W. Runstadler	Pressure recovery performance of straight-channel, single-plane divergence diffusers at high Mach numbers. USAAVLABS Technical Report 69-56, 1969
6	C. F. McDonald	Study of a lightweight integral regenerative gas turbine for high performance. USSAAVLABS Technical Report 70-39, 1970
7	D. P. Morris R. E. Kenny	High pressure ratio centrifugal compressors for small gas turbine engines. AGARD Conference Proceedings 31 Helicopter Propulsion Systems, June 1968
8	R. C. Dean D. D. Wright P. W. Runstadler	Fluid mechanics analysis of high-pressure-ratio centrifugal compressor data. USAAVLABS Technical Report 69-76, 1970
9	A. D. Welliver J. Acurio	Element design and development of small centrifugal compressors. USAAVLABS Technical Report 67-30, 1967
10	R. C. Dean	The centrifugal compressor. Gas Turbine International March-April and May-June, 1973
11	H. Weyer R. Schodl	Development and testing of techniques for oscillating pressure measurements especially suitable for experimental work in turbo-machinery. Trans ASME Journal of Basic Engineering, December 1971
12	D. Eckardt	Private communication from DFVLR

TABLE I

Main design parameters

Mass flow	1.814 kg/s	
Overall pressure ratio	6.5	
Overall isentropic efficiency	0.8	
Impeller		
Pressure ratio	7.76	
Isentropic efficiency	0.9	
Rotational speed	40,000 rev/min	
Specific speed	68	
Number of full vanes	17	
Number of intervanes	17	
Eye hub diameter	60.96 mm	
Eye shroud diameter	134.62 mm	
Eye shroud relative Mach number	0.966	
Eye hub vane angle	38.1°	
Eye shroud vane angle	60.0°	
Eye shroud incidence	0.8°	
Tip diameter	248.92 mm	
Tip width	5.08 mm	
Tip vane speed	521.4 m/s	
Tip absolute Mach number	1.316	
Work input parameter	0.942	
Diffuser	Original design A1	Redesigned A2
Diameter at vane leading edge	261.37 mm	
Axial width	5.08 mm	
Approach Mach number	1.18	
Number of vanes	41	
Throat width	7.01 mm	8.18 mm
Channel length/throat width	9.00	7.63
Area ratio	2.10	1.83
Diameter at vane trailing edge	354.00 mm	

TABLE II

Summary of builds

Build No.	Impeller	Diffuser	Collector	Purpose
I	Design with static shroud clearance of 400 μm approximately	Vaneless	Design	Mechanical and instrumentation checks, mainly establishment of required impeller shroud clearance
II	Design with static shroud clearance increased by 150 μm axially	Vaneless	Design	
III	Design with static shroud clearance further increased by 100 μm axially	Vaneless	Design	Performance evaluation of design impeller
IV	As Build III	Design vaned, A1	Design	Performance evaluation of design compressor stage
V	Modified; i.e. design with leading edge of vanes cut back axially by 5.08 mm	Vaneless	Design	Performance evaluation of modified impeller
VI	As Build V	Redesigned vaned, A2	Design	Performance evaluation of modified compressor stage
VII	As Build V	A2	Redesigned	Performance evaluation of modified compressor stage with redesigned collector

TABLE III

Build III derived parameters

Corrected speed rev/min	20,000	25,000	29,000	32,000	34,000	36,000	38,000	40,000
Corrected mass flow kg/s	0.541	0.643	0.884	1.096	1.281	1.380	1.471	1.498
Impeller pressure ratio	1.831	2.454	3.187	3.952	4.505	5.197	6.148	6.841
Impeller total-to-total isentropic efficiency	0.877	0.861	0.866	0.865	0.853	0.851	0.843	0.826
Eye shroud relative Mach number*	0.429	0.536	0.632	0.710	0.767	0.815	0.865	0.908
Tip absolute Mach number*	0.691	0.830	0.943	1.035	1.095	1.139	1.197	1.217
Work input parameter	0.916	0.925	0.918	0.924	0.927	0.926	0.949	0.940
Flow range per cent	-	-	-	-	-	22.3	18.3	17.2

* Derivation given in Appendix B

TABLE IV

Build V derived parameters

Corrected speed rev/min	20,000	25,000	32,000	36,000	38,000	40,000
Corrected mass flow kg/s	0.582	0.659	1.033	1.364	1.449	1.499
Impeller pressure ratio	1.762	2.371	3.845	5.148	5.943	6.905
Impeller total-to-total isentropic efficiency	0.858	0.844	0.847	0.840	0.835	0.820
Eye shroud relative Mach number	0.435	0.538	0.704	0.814	0.861	0.890
Tip absolute Mach number	0.672	0.816	1.018	1.136	1.177	1.227
Work input parameter	0.873	0.903	0.921	0.932	0.936	0.953
Flow range per cent	-	-	-	24.8	21.8	20.9

TABLE V

Build VI derived parameters

Corrected speed rev/min	32,000	36,000	38,000	40,000
Corrected mass flow kg/s	1.124	1.422	1.597	1.755
Overall pressure ratio	3.290	4.259	4.961	5.282*
Overall total-to-total isentropic efficiency	0.751	0.740	0.745	0.699
Eye shroud relative Mach number	0.713	0.821	0.881	0.940
Tip absolute Mach number	1.013	1.146	1.242	1.308
Diffuser exit Mach number**	0.355	0.365	0.360	0.384
Work input parameter	0.905	0.927	0.934	0.942
Diffuser total pressure ratio	0.792	0.800	0.860	0.804
Diffuser static pressure recovery coefficient†	0.500	0.487	0.516	0.447
Flow range per cent	11.9	6.3	4.1	3.2

* pressure ratio significantly below maximum
** derivation given in Appendix B
† assumes blockage of 0.1 at throat

TABLE VI

Build VII derived parameters

Corrected speed rev/min	20,000	25,000	32,000	36,000	38,000	40,000
Corrected mass flow kg/s	0.552	0.678	1.036	1.327	1.470	1.600
Overall pressure ratio	1.724	2.273	3.511	4.580	5.219	5.913
Overall total-to-total isentropic efficiency	0.799	0.790	0.785	0.776	0.764	0.746
Overall total-to-static isentropic efficiency	0.696	0.728	0.739	0.733	0.725	0.712
Eye shroud relative Mach number	0.432	0.539	0.705	0.810	0.864	0.919
Tip absolute Mach number	0.684	0.824	1.008	1.116	1.178	1.224
Diffuser exit Mach number	0.289	0.282	0.302	0.312	0.311	0.306
Work input parameter	0.903	0.913	0.918	0.924	0.934	0.945
Diffuser total pressure ratio	0.921	0.898	0.824	0.817	0.832	0.783
Diffuser static pressure recovery coefficient†	0.475	0.570	0.609	0.610	0.626	0.658
Flow range per cent	-	22.2	19.0	16.2	14.0	12.2

† assumes blockage of 0.1 at throat

TABLE VII

Comparison of test and predicted efficiencies

Build	Station	Isentropic (total-to-total) efficiency at 40,000 rev/min and 1.7 kg/s	Efficiency difference	
			Test	Predicted
V Modified impeller with vaneless diffuser	Impeller tip (124.46 mm radius)	0.843	0.049	0.055
	Vaneless diffuser (133.35 mm radius)	0.794		
VII Modified impeller with vaned diffuser	Compressor overall (Vaned diffuser exit)	0.743	0.051	

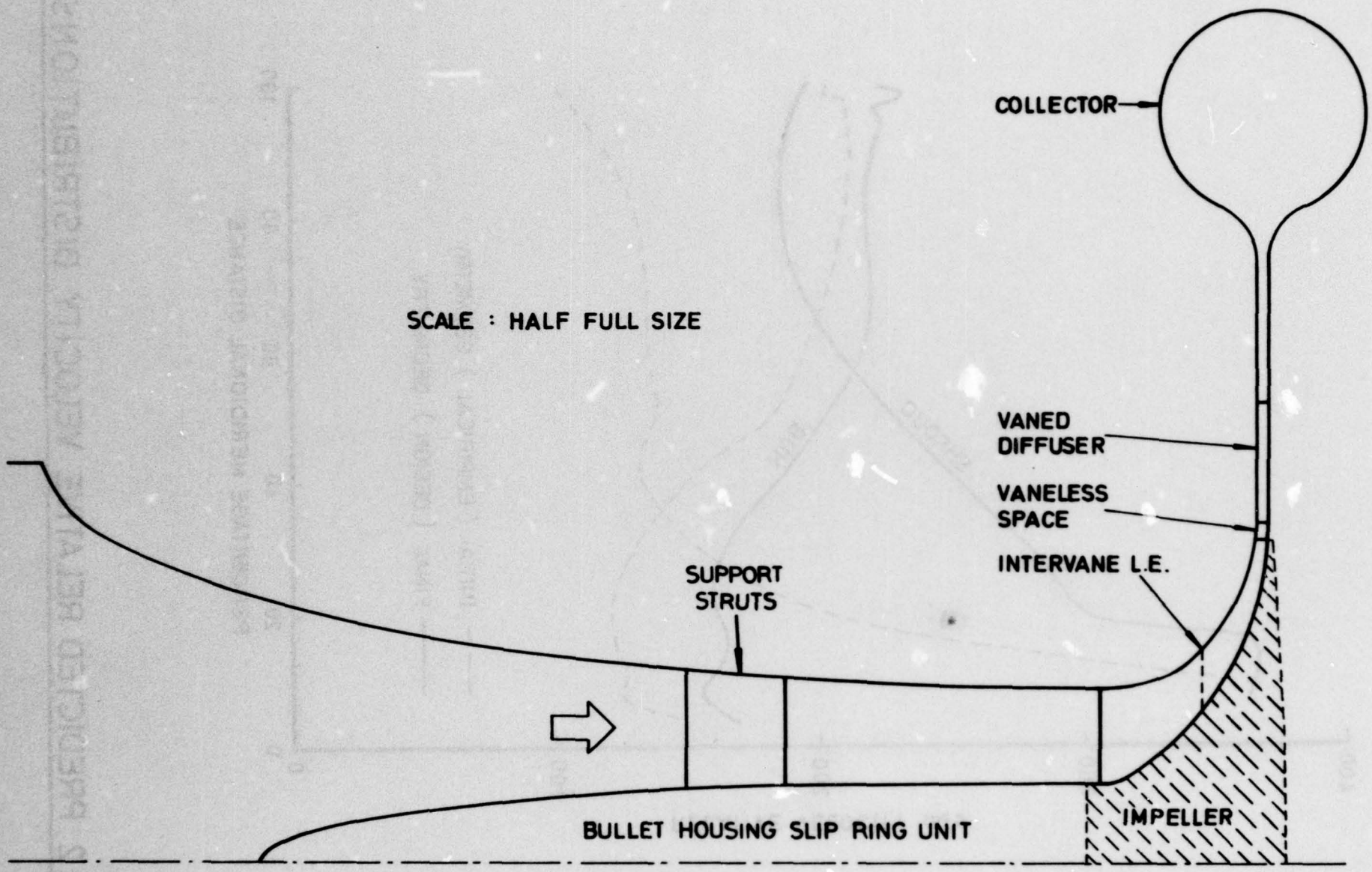

FIG.1 LAYOUT OF COMPRESSOR

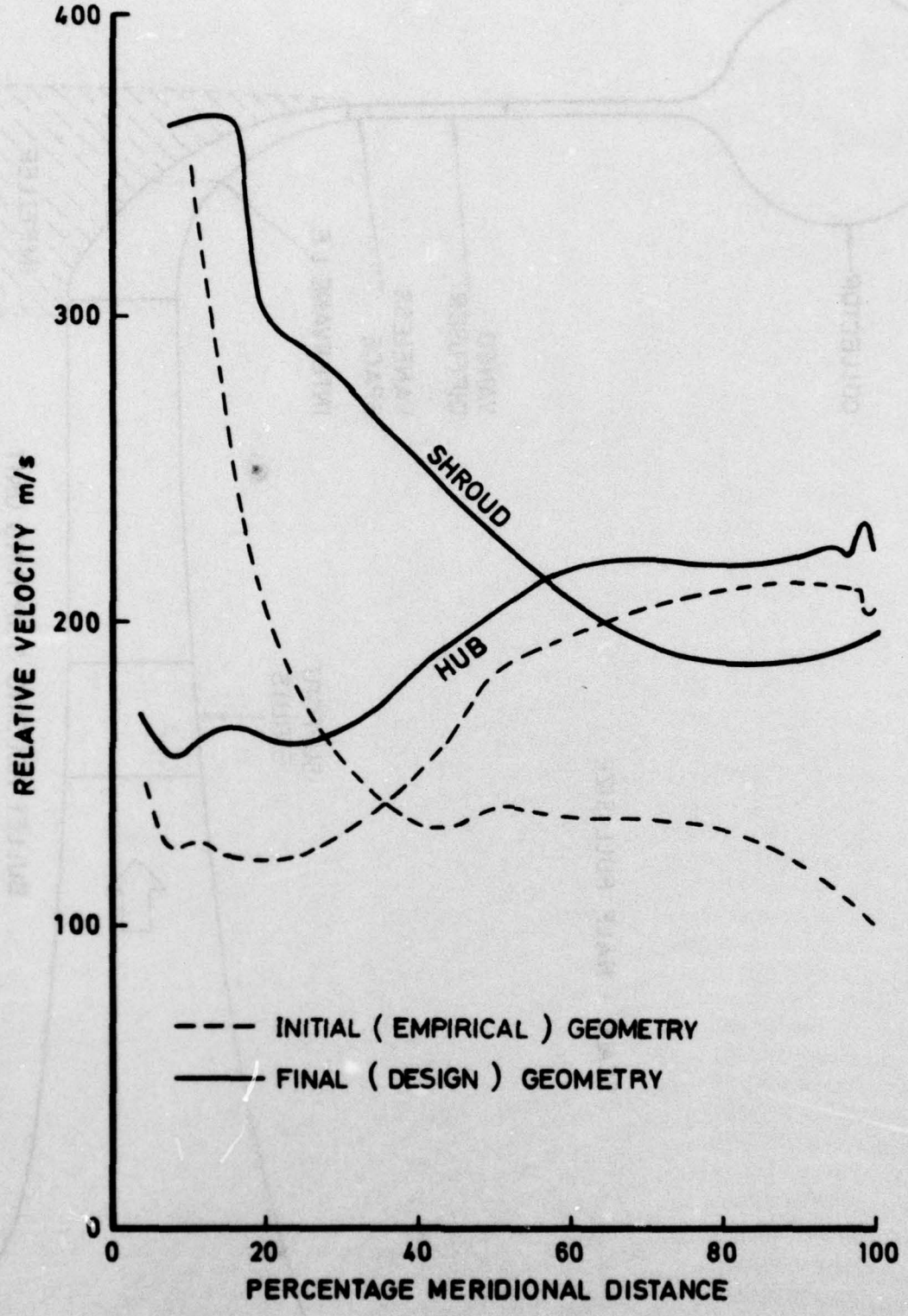

FIG. 2 PREDICTED RELATIVE VELOCITY DISTRIBUTIONS

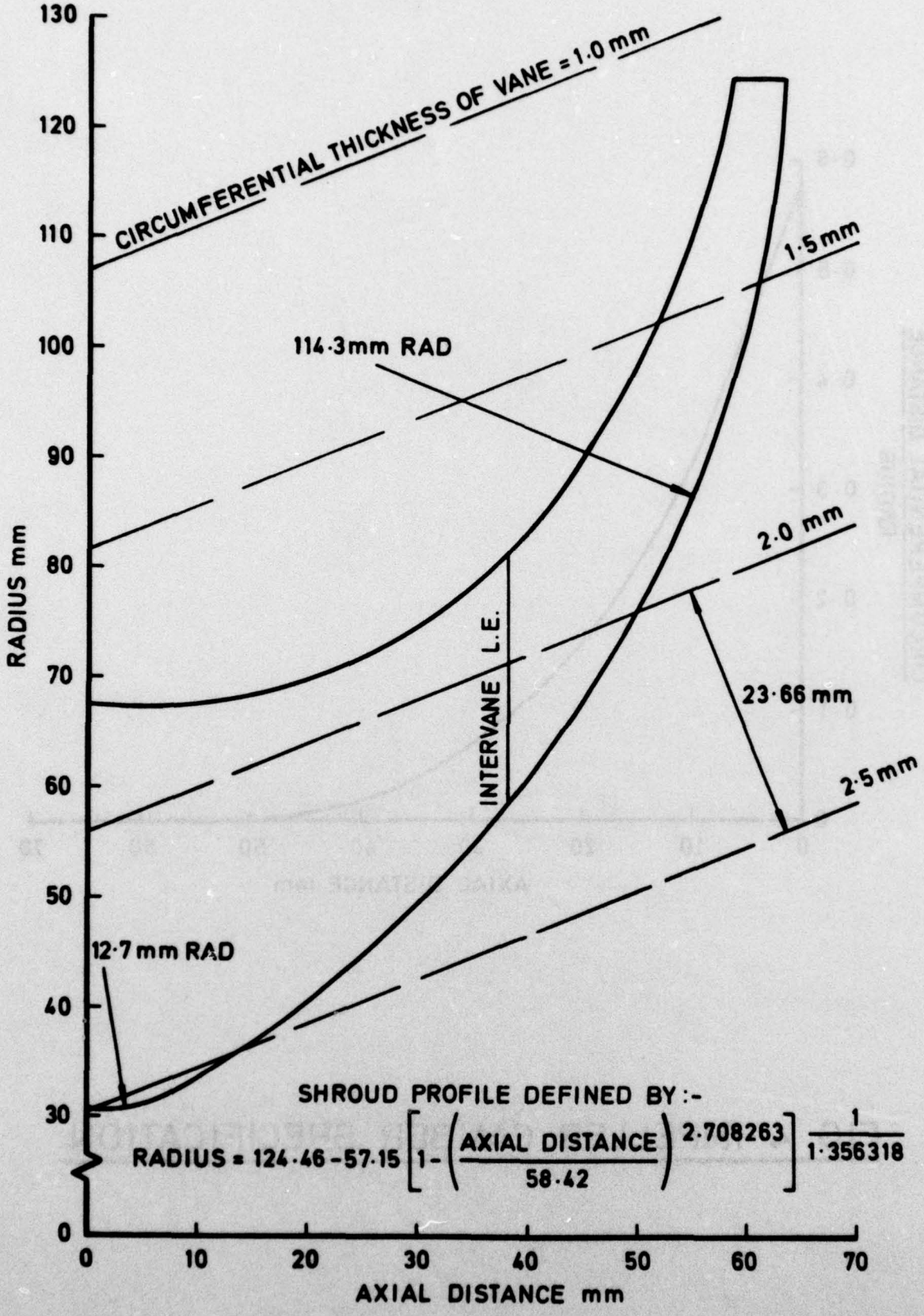

FIG. 3 IMPELLER MERIDIONAL SHAPE AND VANE THICKNESS

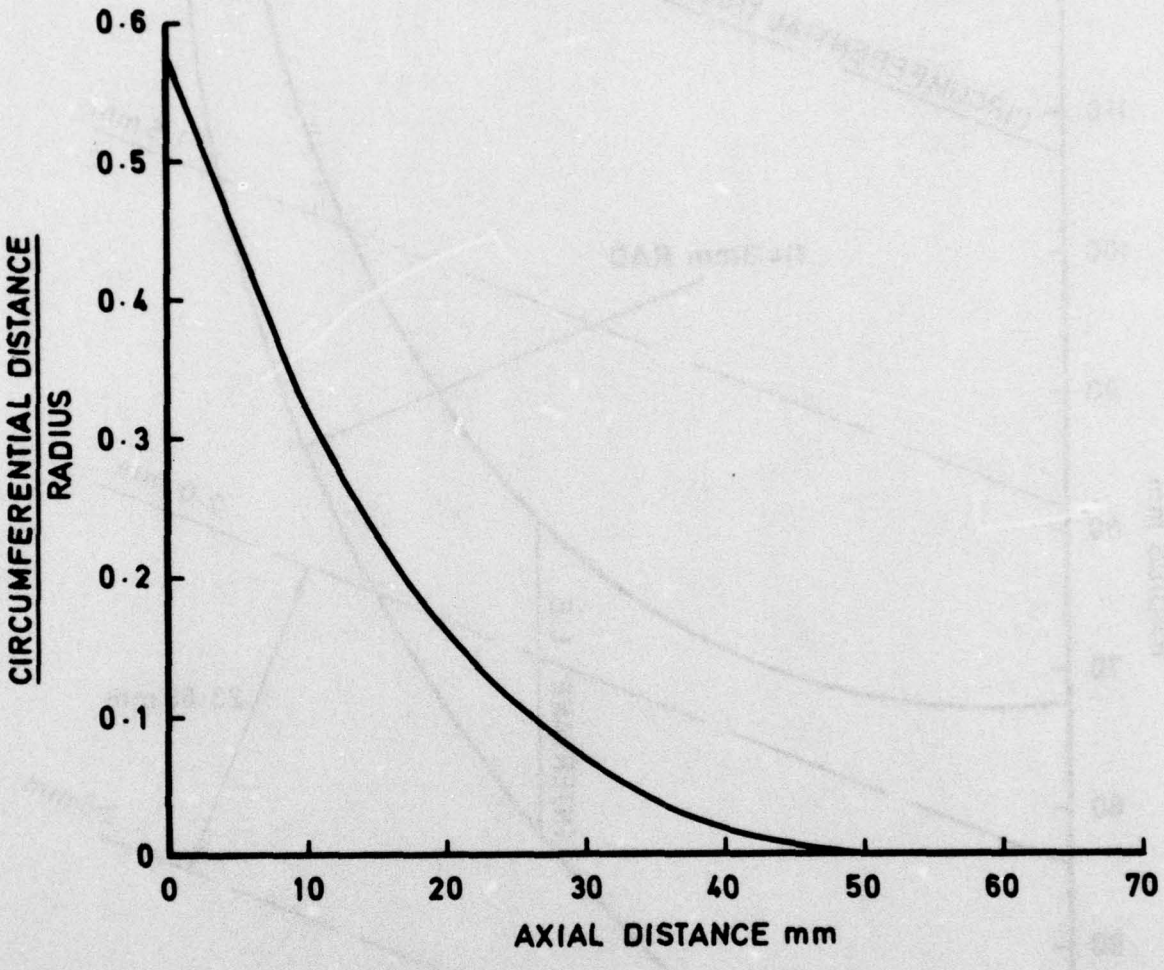

FIG. 4 IMPELLER CAMBER SPECIFICATION

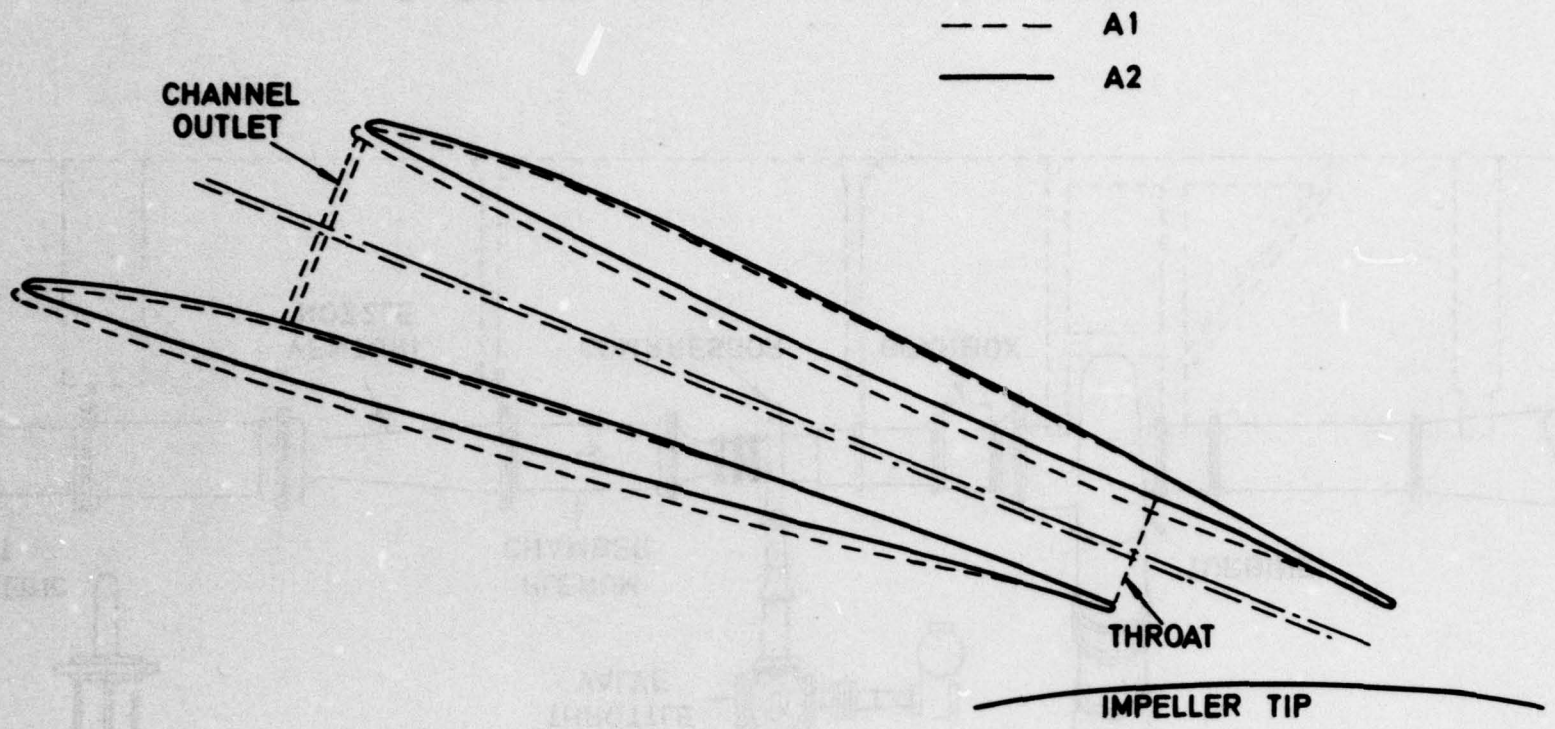

FIG.5 VANED DIFFUSER GEOMETRY

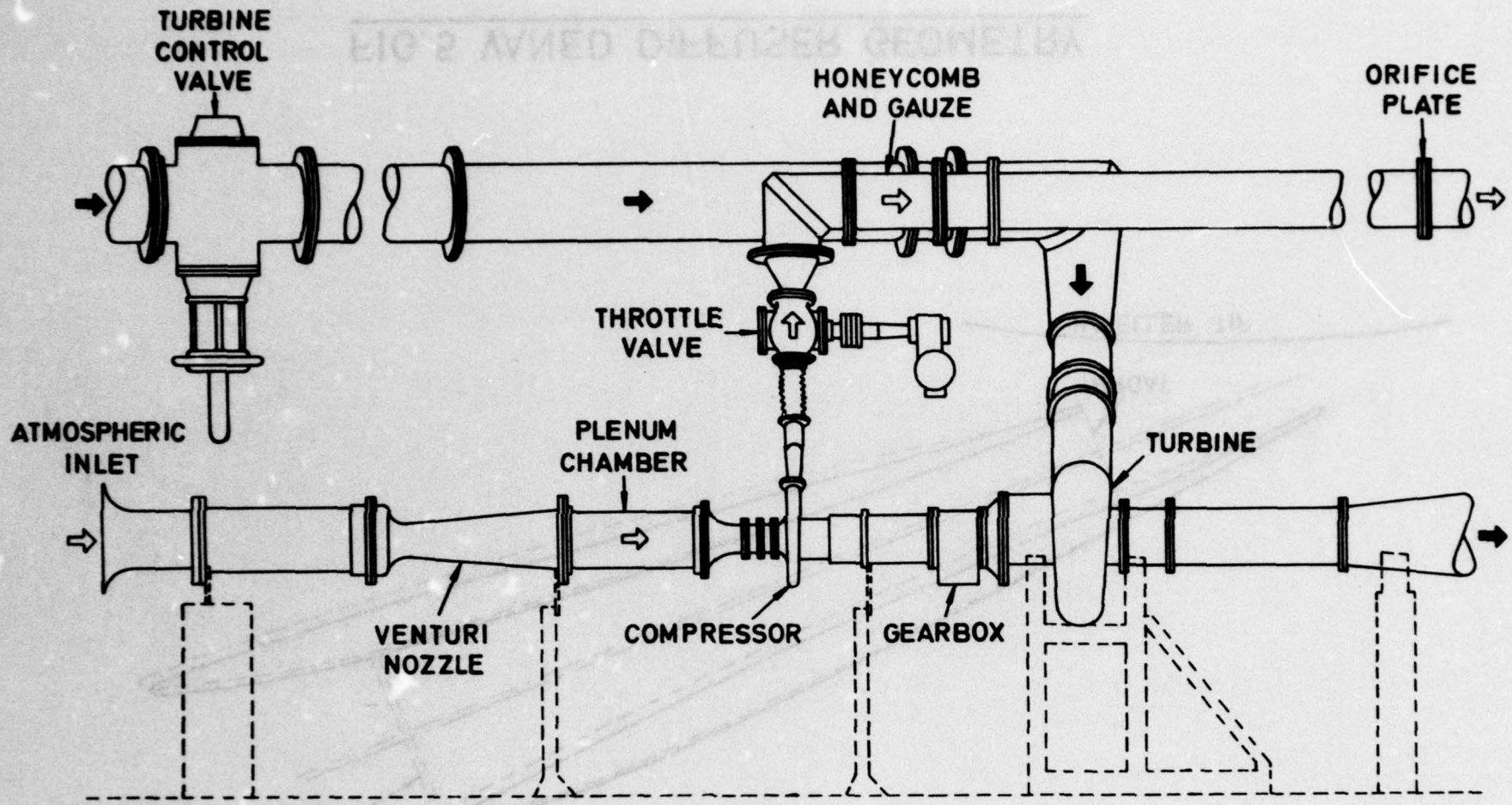

FIG. 6 SCHEMATIC LAYOUT OF TEST RIG

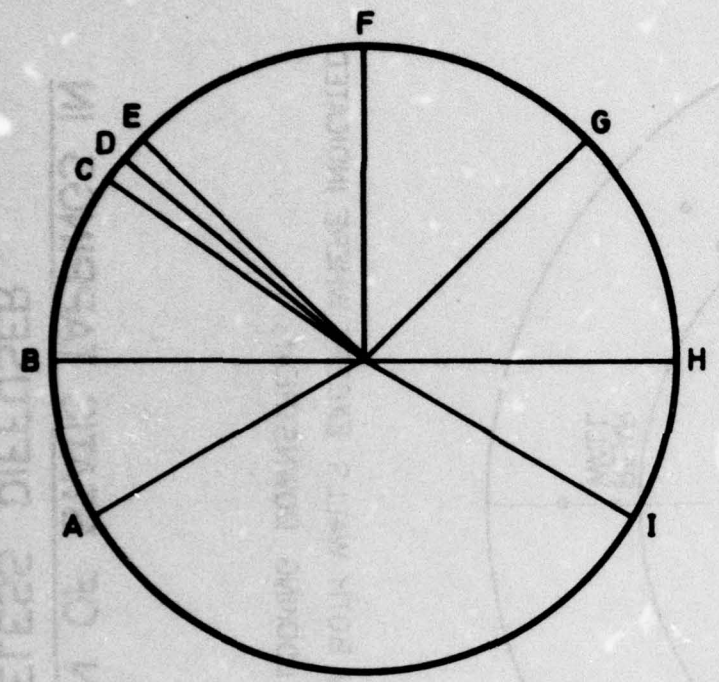

NOMENCLATURE OF RADIAL PLANES CONTAINING TAPPINGS

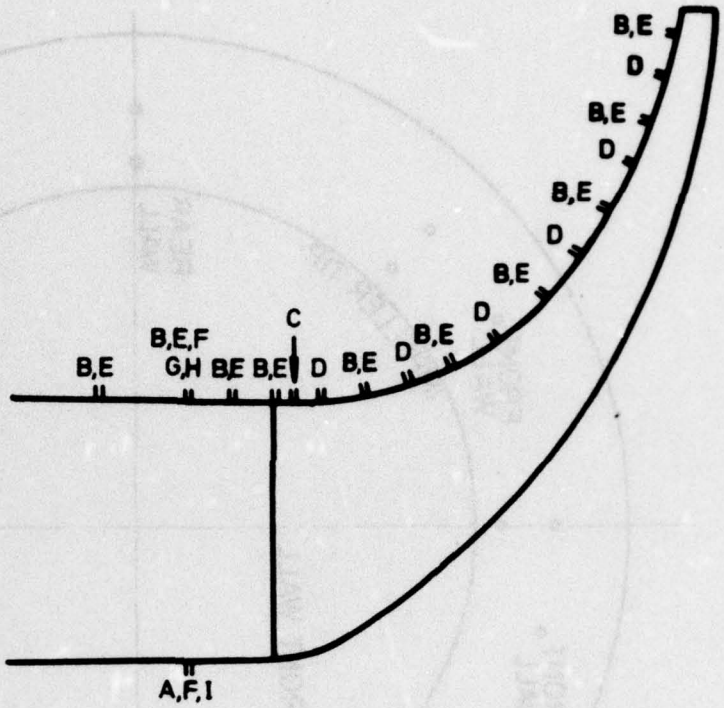

SCALE : FULL SIZE

FIG.7 LOCATION OF STATIC TAPPINGS IN IMPELLER INLET AND SHROUD CASING

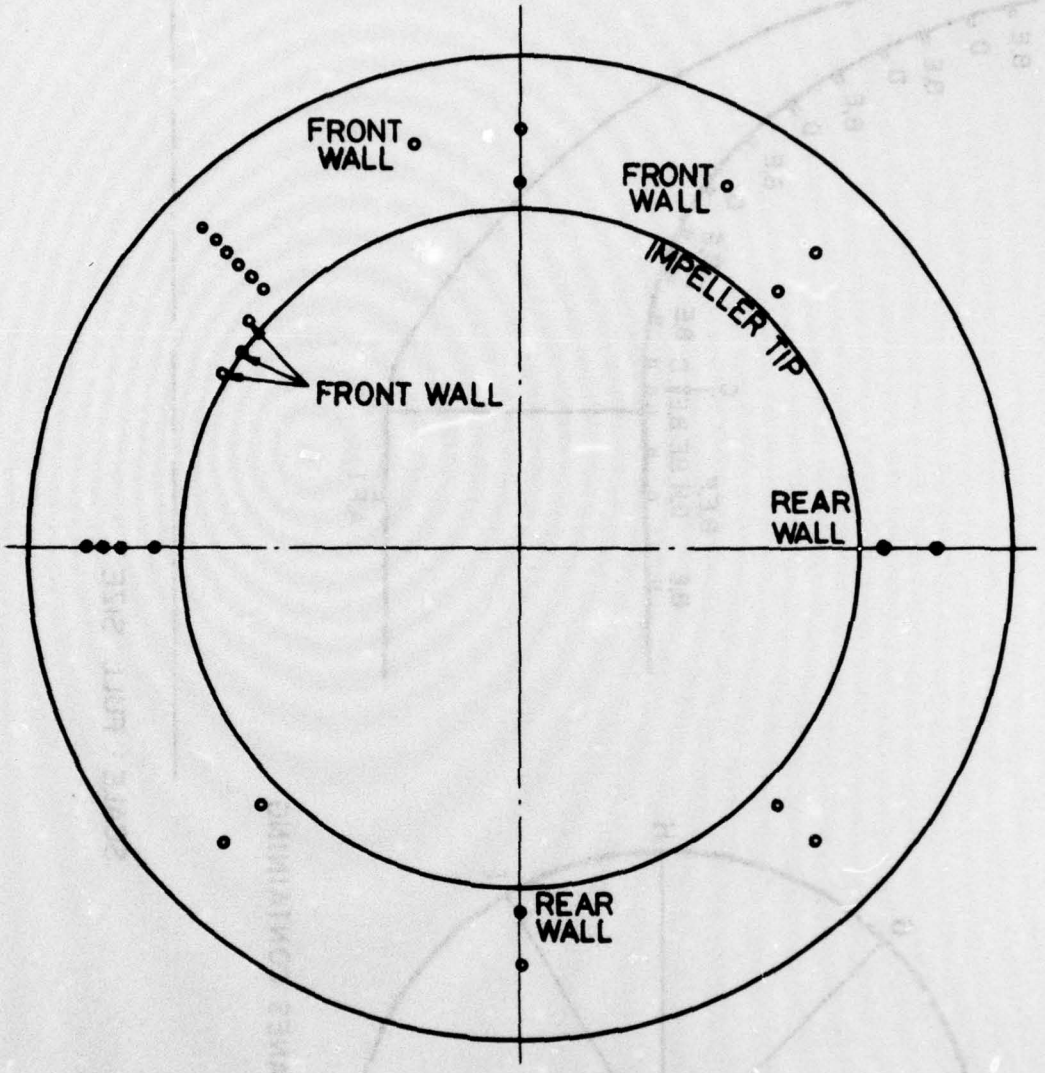

ALL TAPPINGS ON BOTH WALLS EXCEPT WHERE INDICATED

LOOKING DOWNSTREAM

FIG. 8 LOCATION OF STATIC TAPPINGS IN VANELESS DIFFUSER

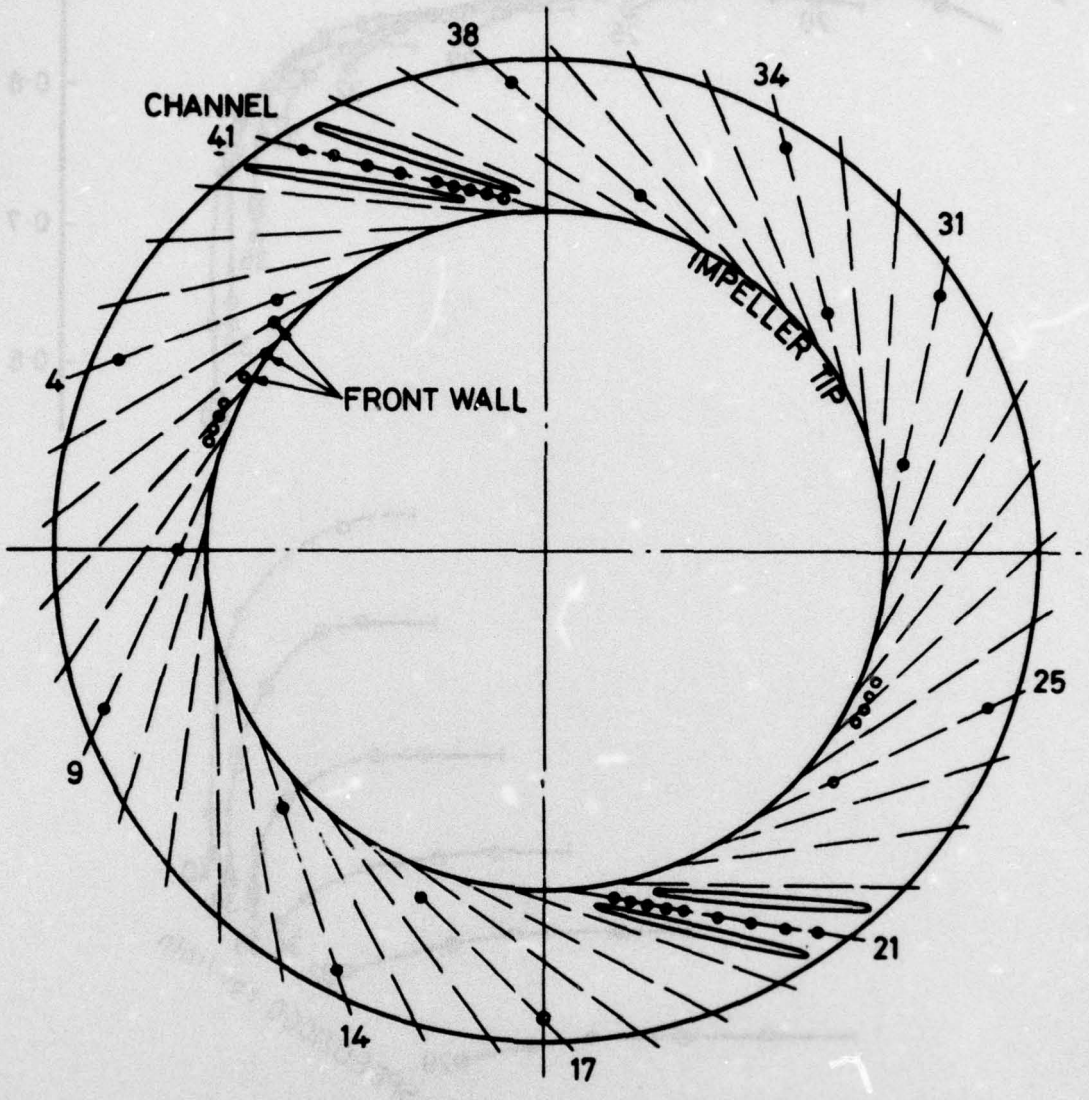

ALL TAPPINGS ON REAR WALL EXCEPT WHERE INDICATED

LOOKING DOWNSTREAM

FIG 9 LOCATION OF STATIC TAPPINGS IN A2 VANED DIFFUSER

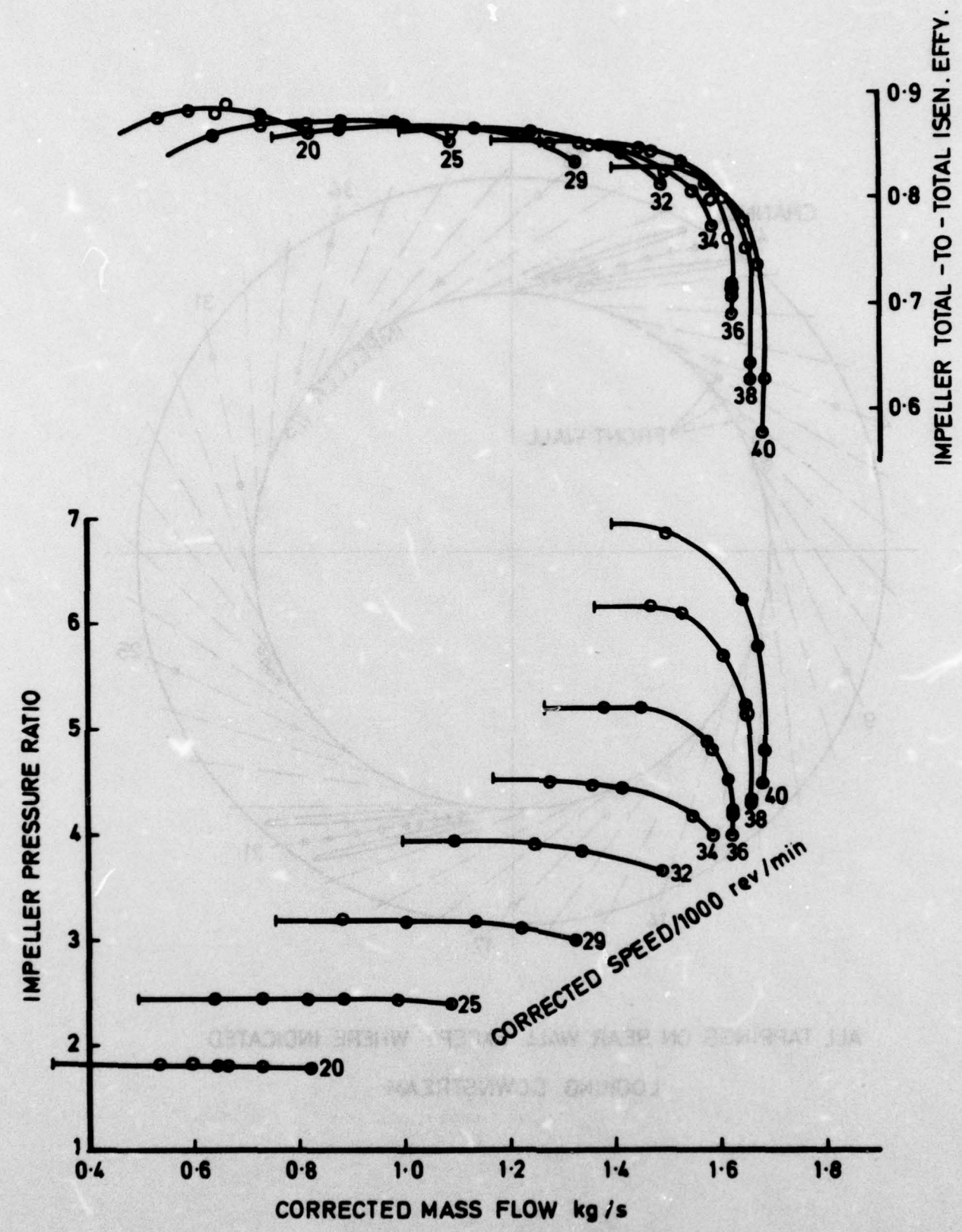

FIG. 10 BUILD III IMPELLER CHARACTERISTIC

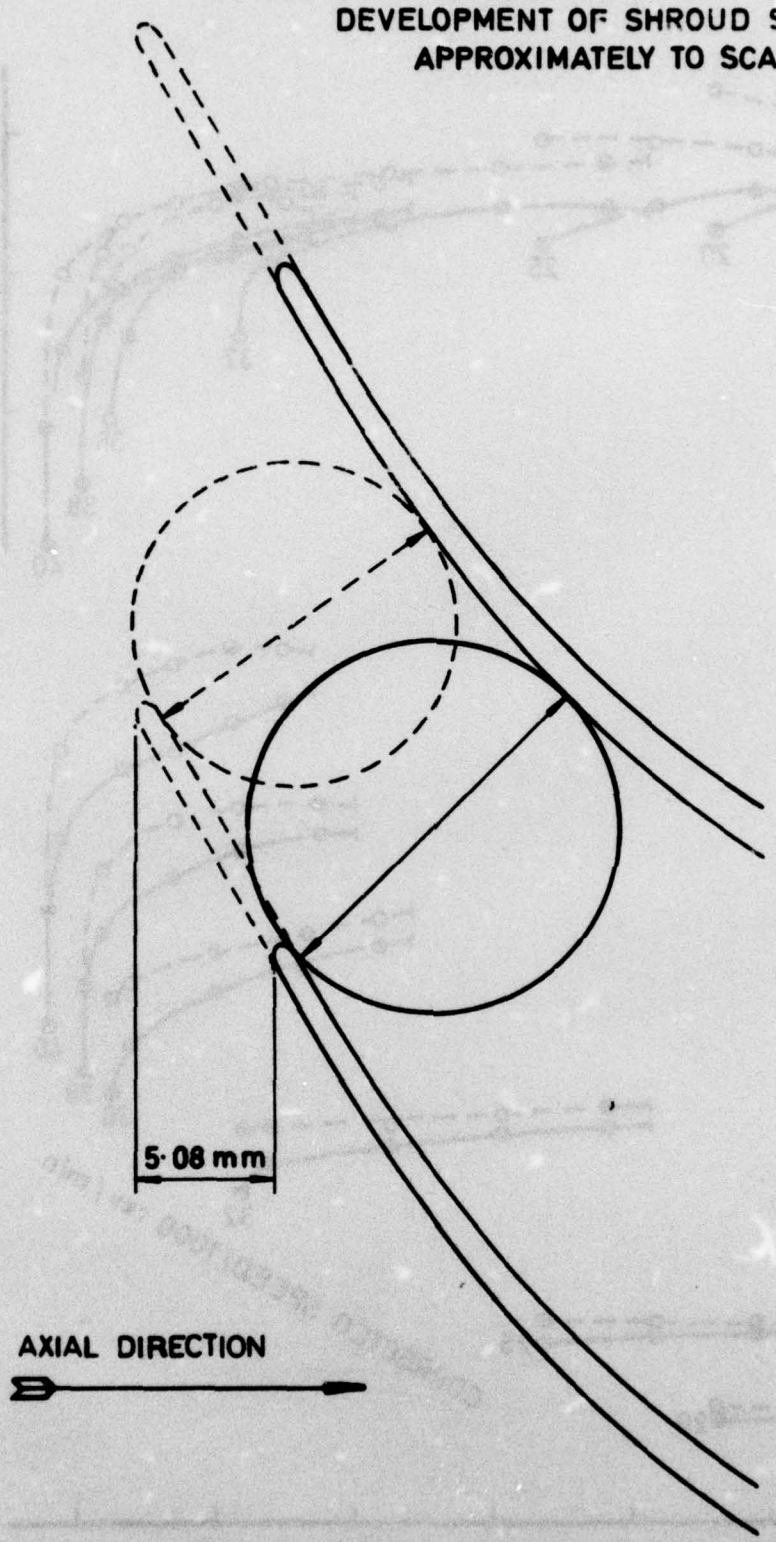

FIG.11 CUT-BACK OF IMPELLER VANE LEADING EDGES

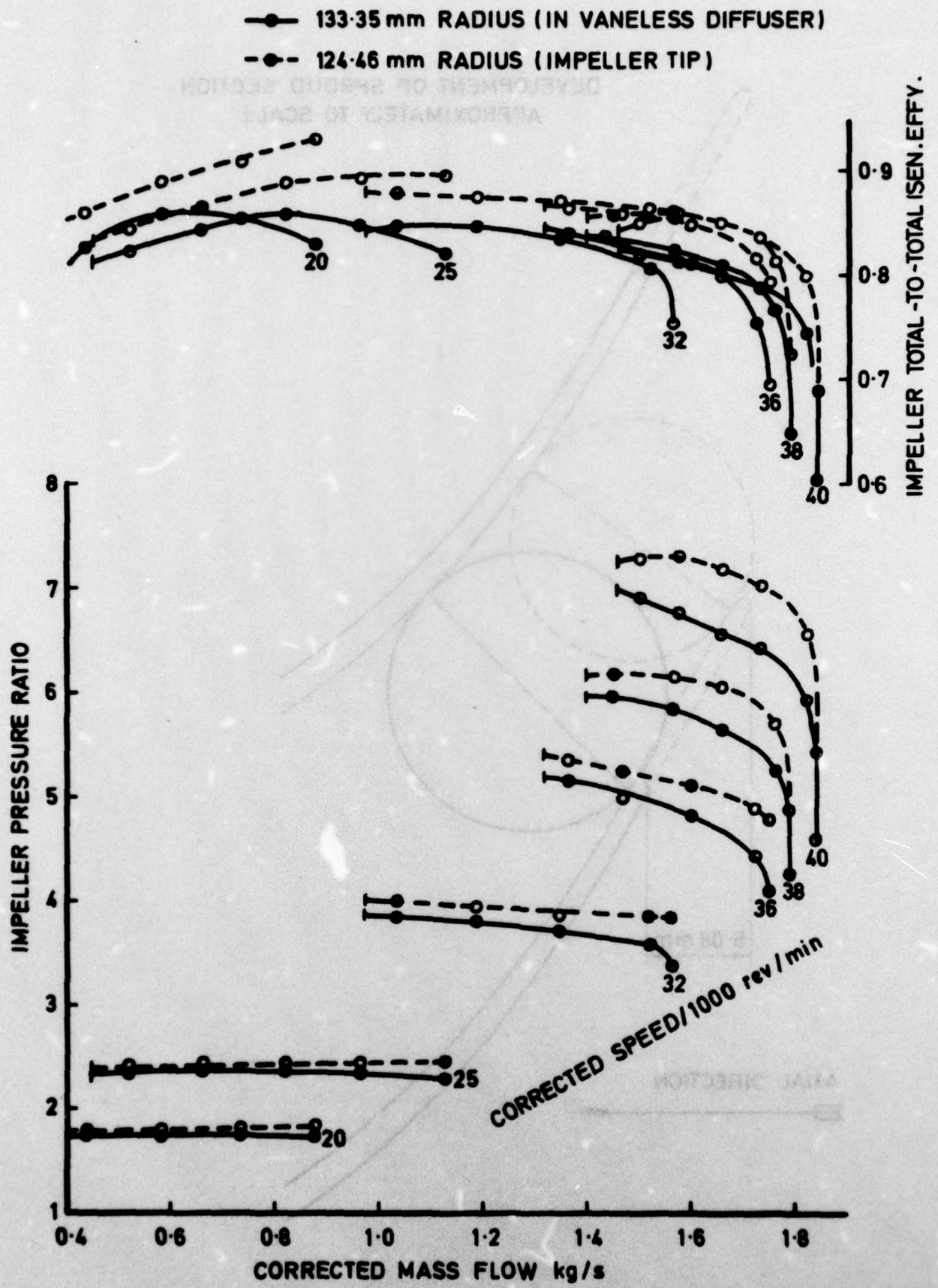

FIG. 12 BUILD V IMPELLER CHARACTERISTIC

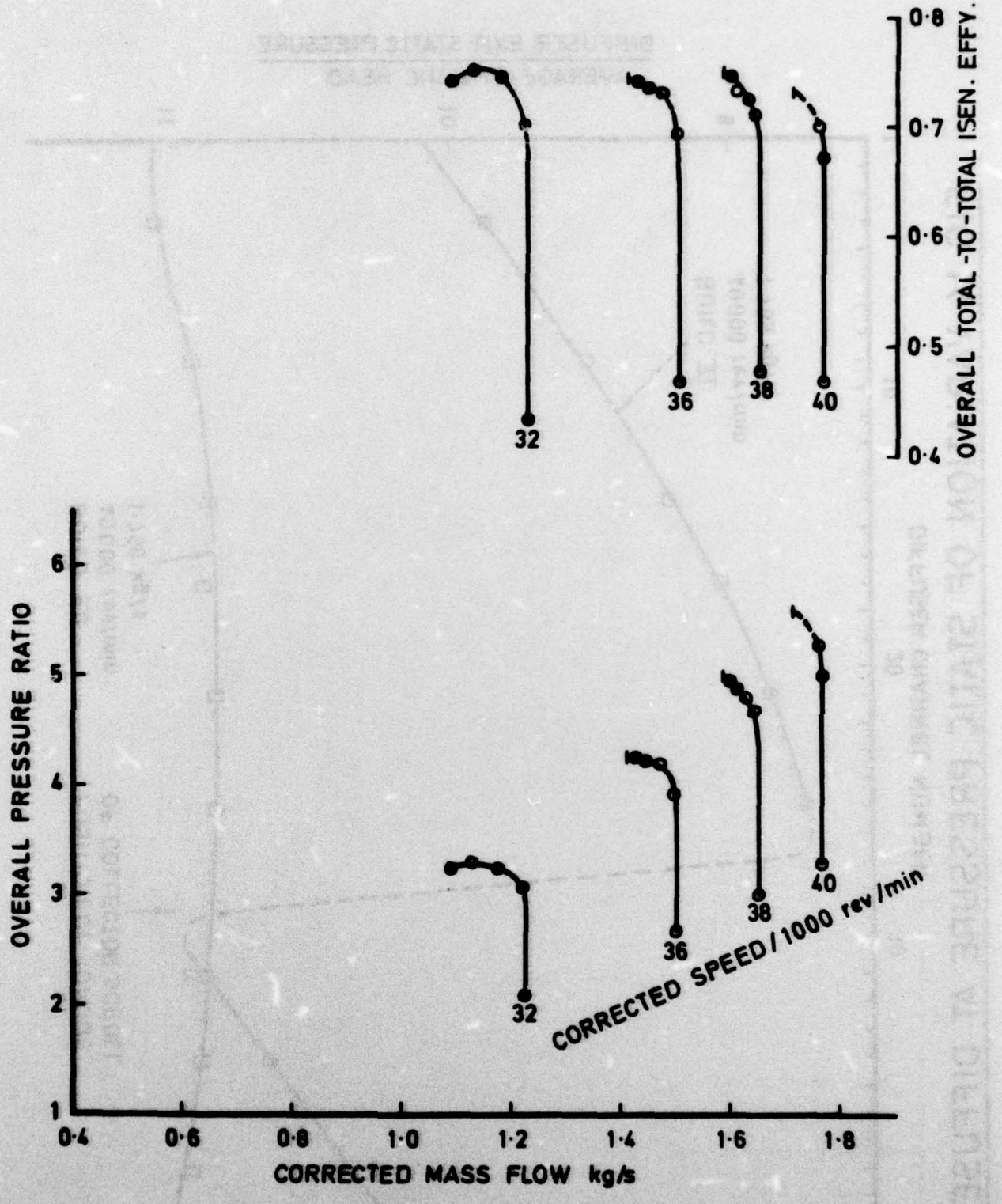

FIG.13 BUILD VI OVERALL CHARACTERISTIC

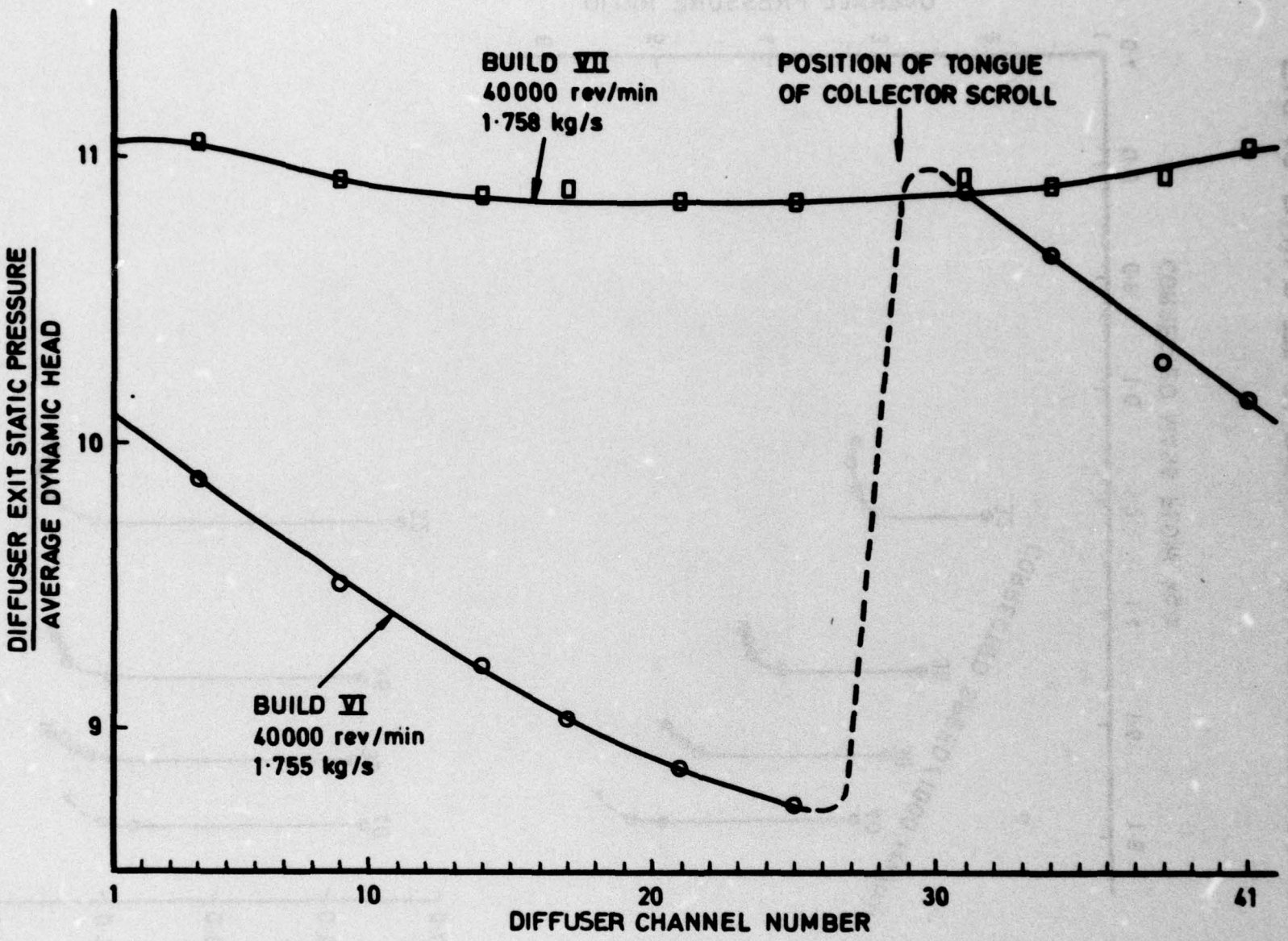

FIG. 14 VARIATION OF STATIC PRESSURE AT DIFFUSER EXIT

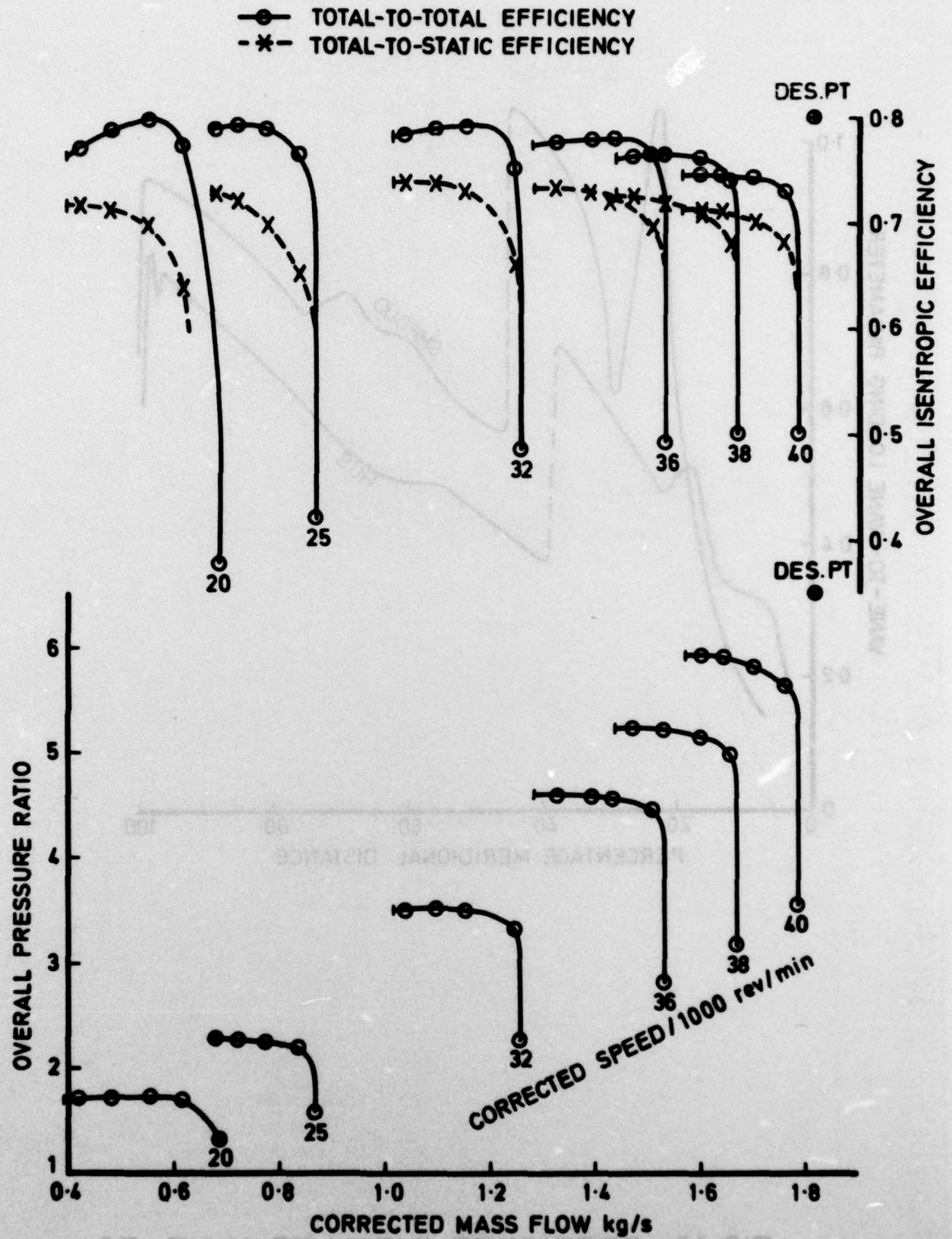

FIG. 15 BUILD VII OVERALL CHARACTERISTIC

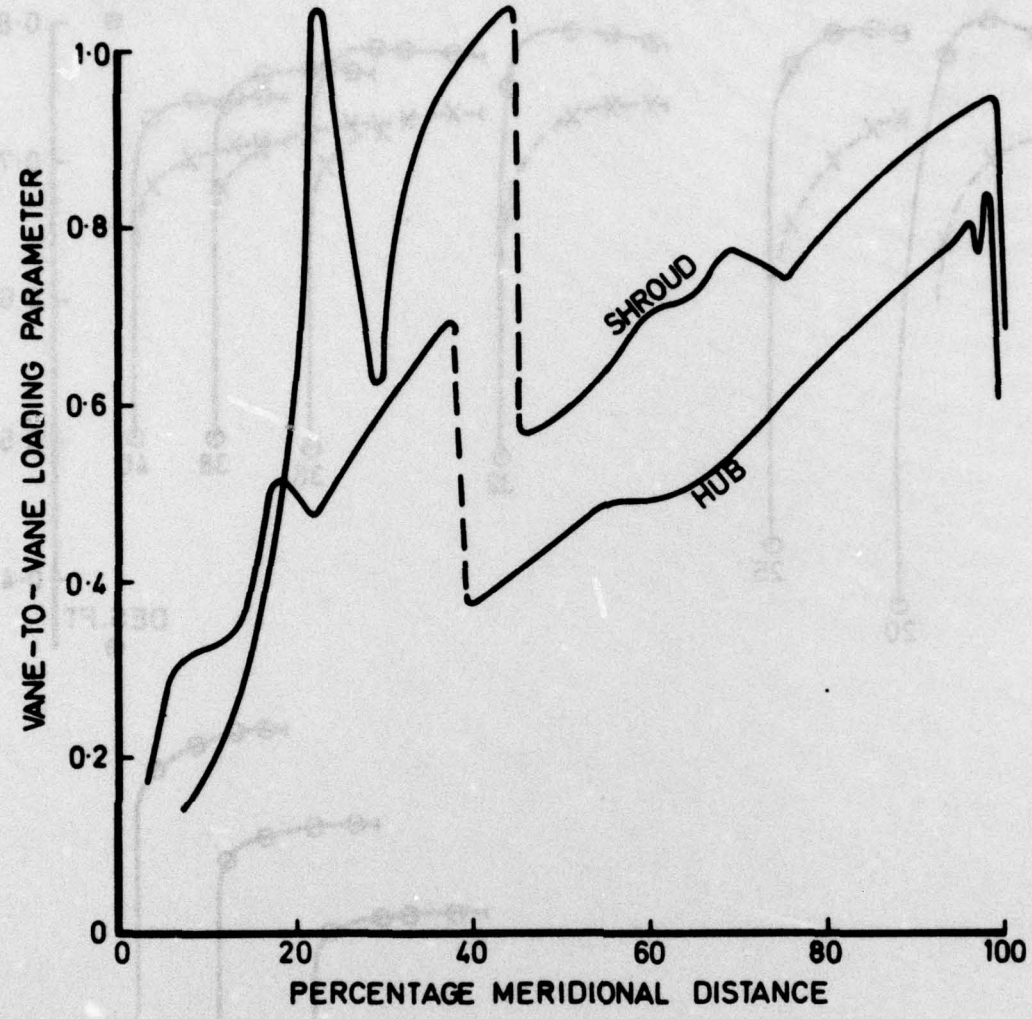

FIG.16 PREDICTED IMPELLER VANE-TO-VANE LOADING DISTRIBUTIONS

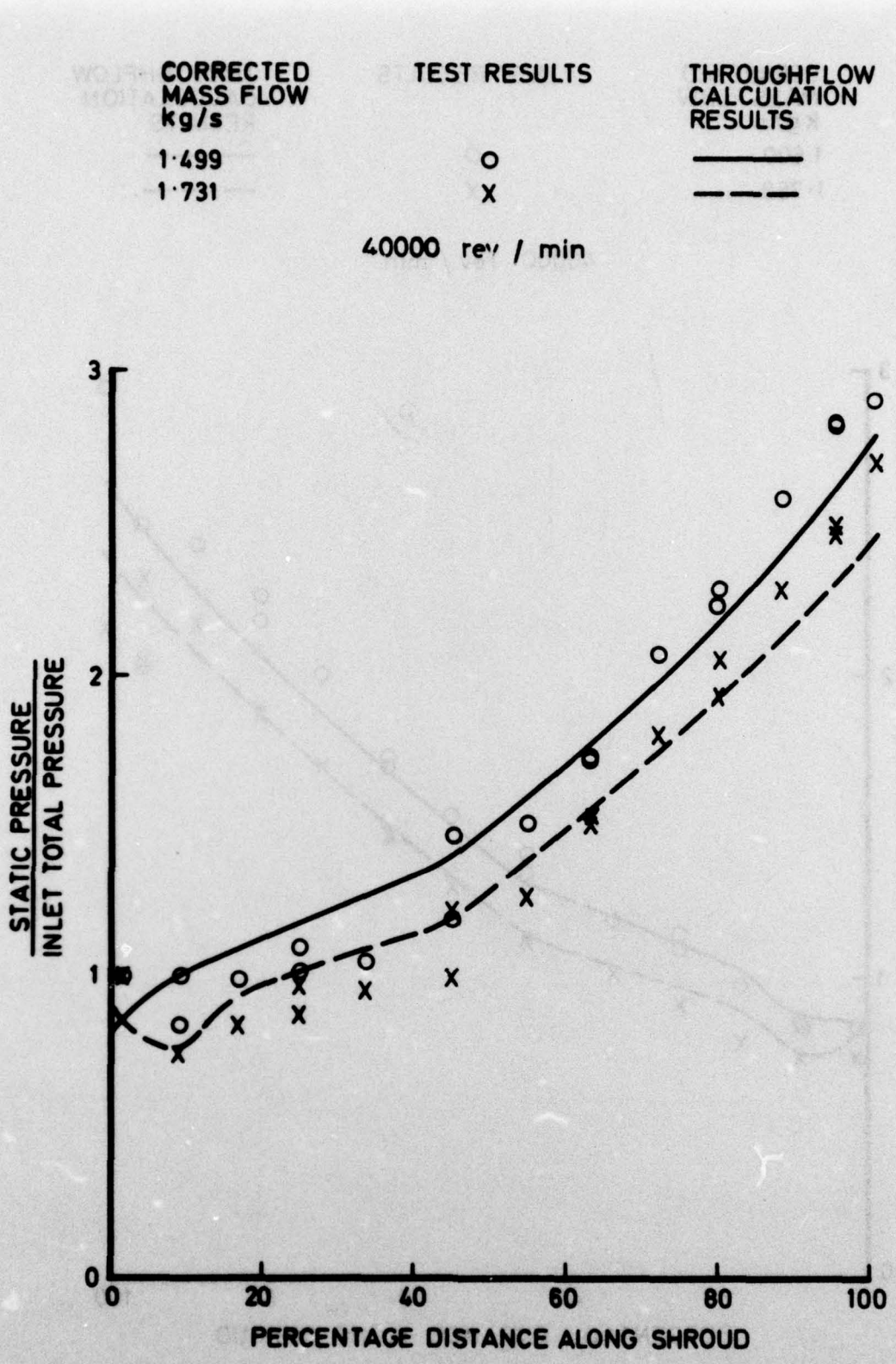

FIG.17 BUILD V IMPELLER SHROUD STATIC PRESSURES

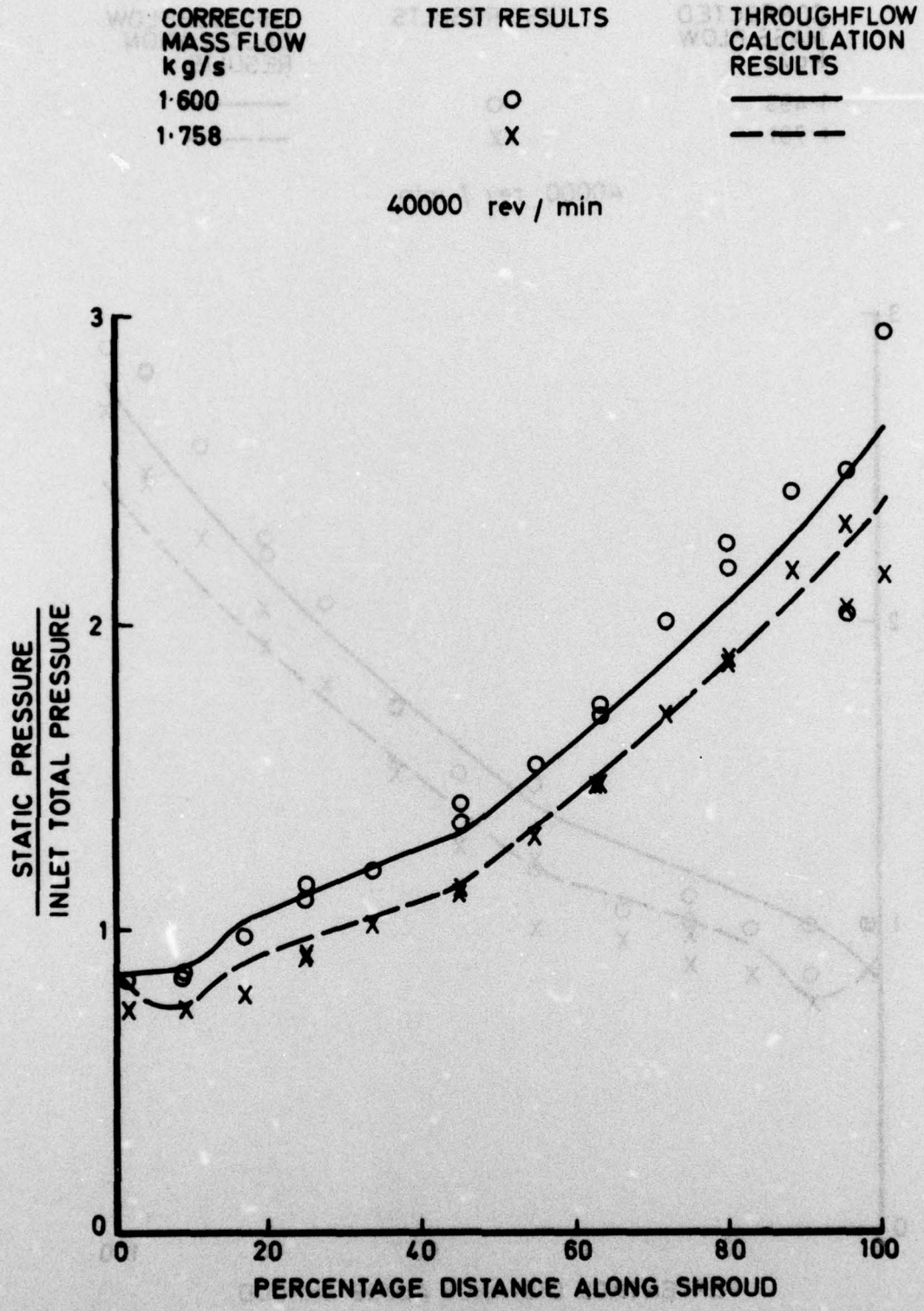

FIG. 18 BUILD VII IMPELLER SHROUD STATIC PRESSURES

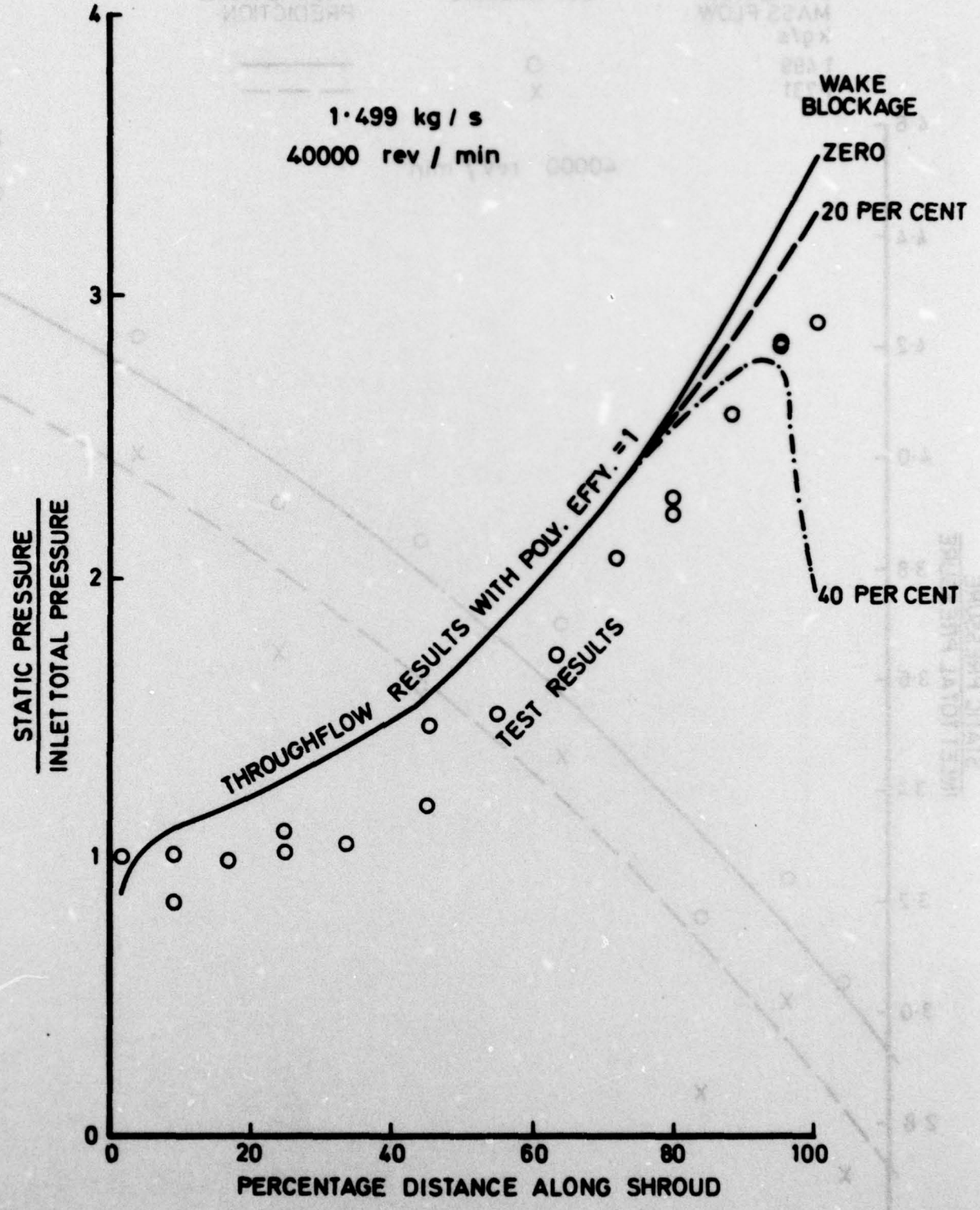

FIG. 19 BUILD V IMPELLER SHROUD STATIC PRESSURES FOR JET/WAKE MODEL

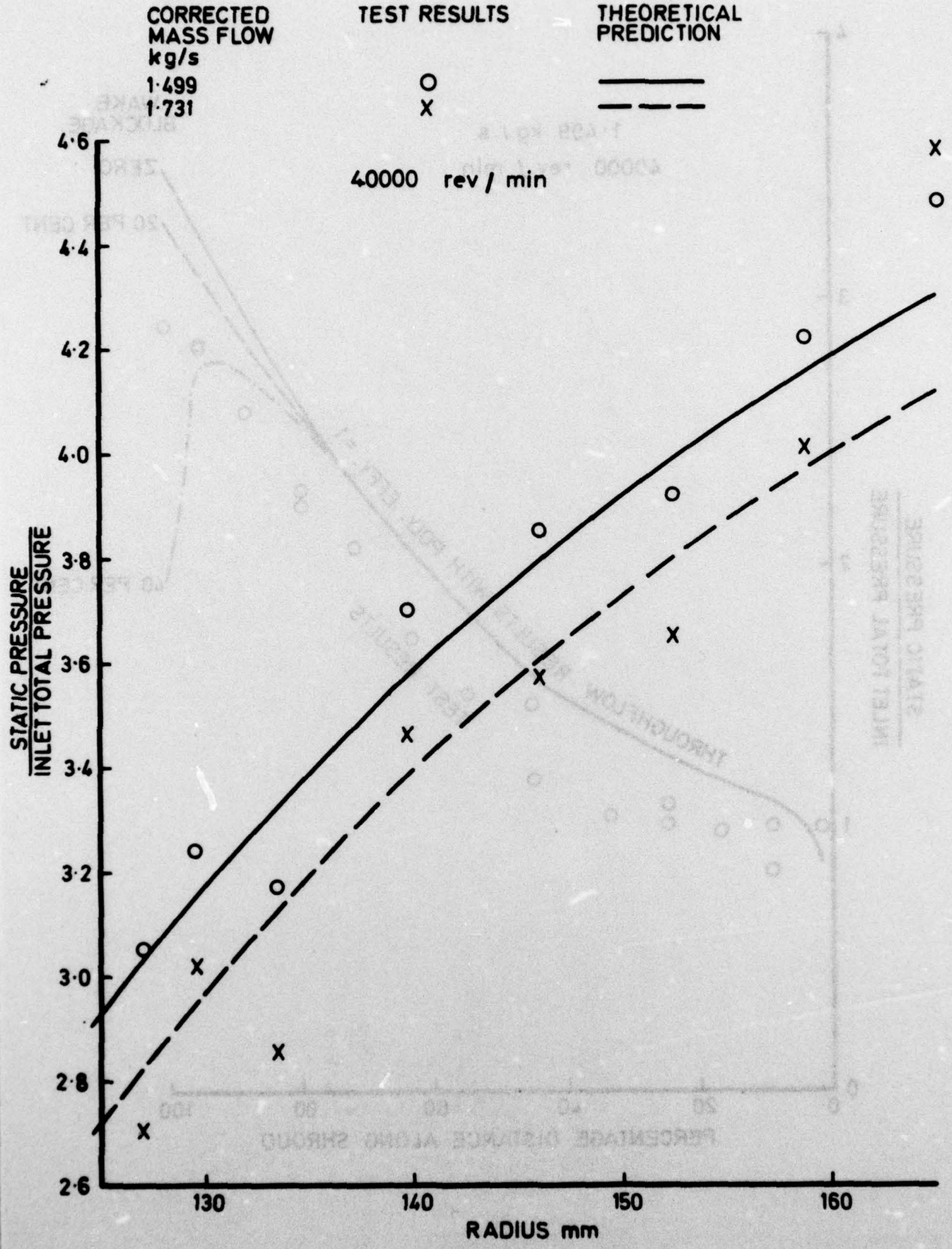

FIG. 20 BUILD V VANELESS DIFFUSER STATIC PRESSURES

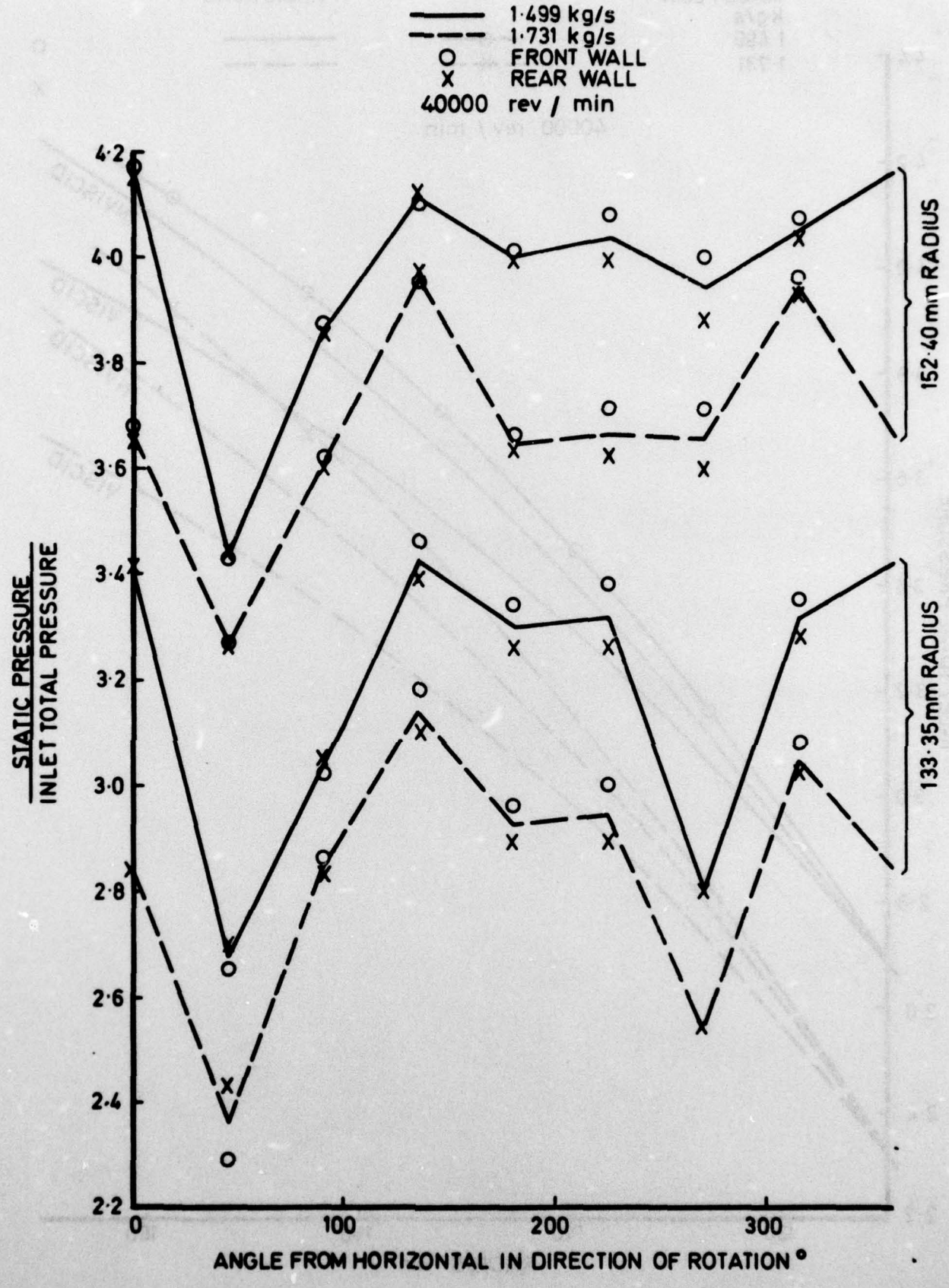

FIG. 21 BUILD V VANELESS DIFFUSER CIRCUMFERENTIAL STATIC PRESSURE DISTRIBUTIONS

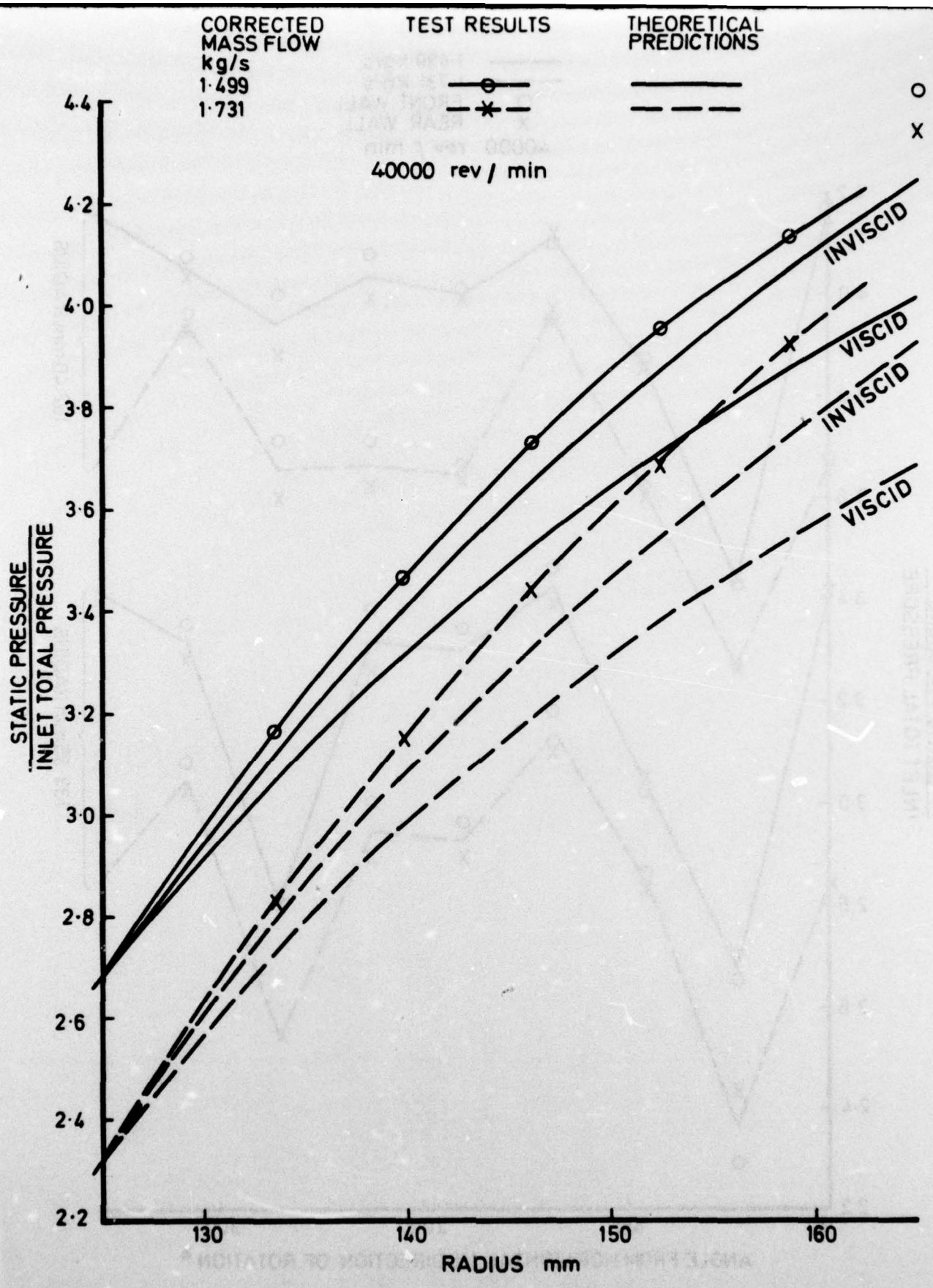

FIG.22 BUILD V VANELESS DIFFUSER AREA-WEIGHTED MEAN STATIC PRESSURES

Produced in England by Her Majesty's Stationery Office, Reprographic Centre, Basildon

Bas 41602/587483 K5 10/77 TPQ3

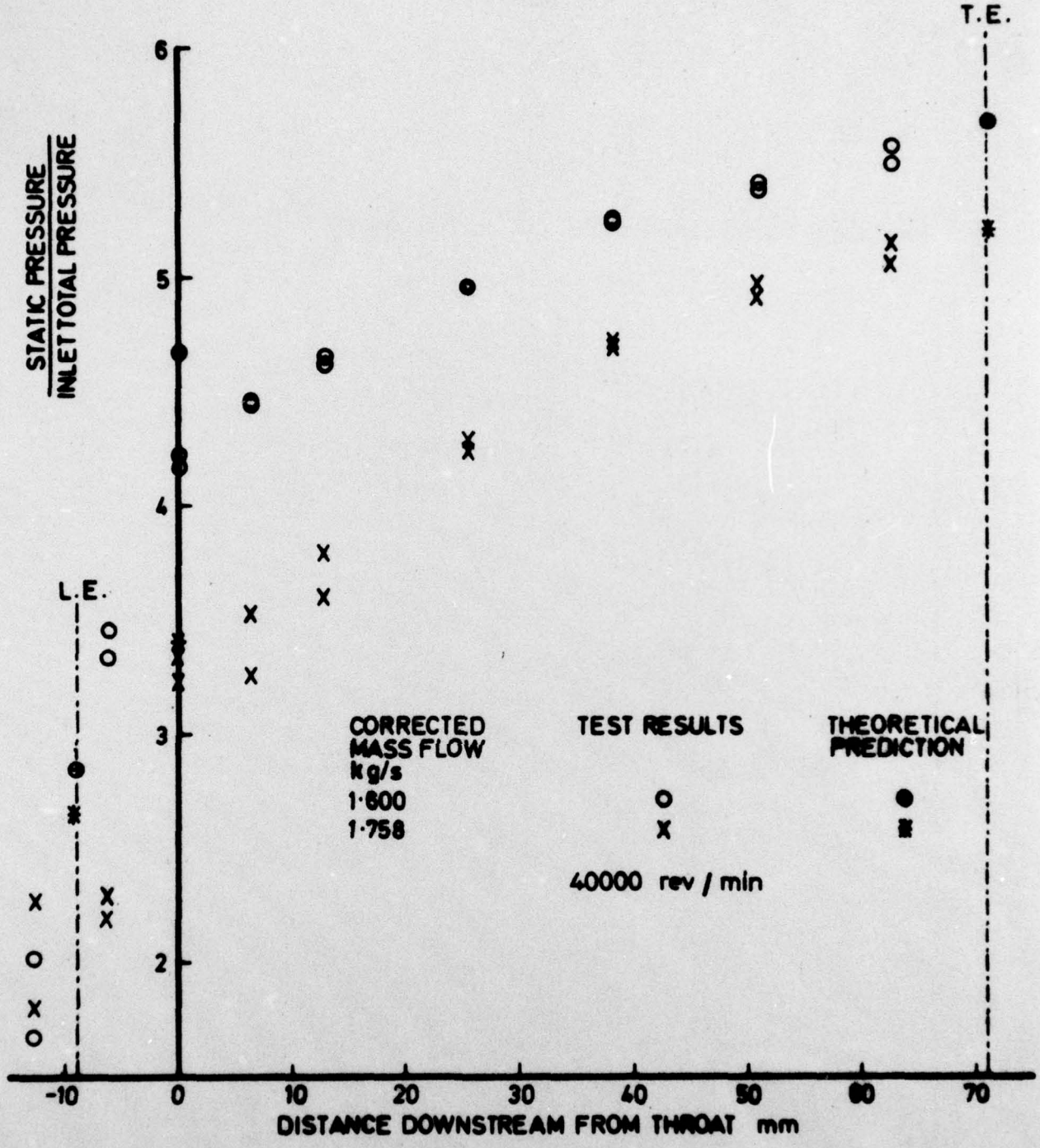

FIG. 23 BUILD VII VANED DIFFUSER STATIC PRESSURES ON CHANNEL CENTRE-LINE

DETACHABLE ABSTRACT CARDS

ARC CP No.1385
September 1976
Jones, M.G.

THE PERFORMANCE OF A 6.5 PRESSURE RATIO CENTRIFUGAL COMPRESSOR HAVING A RADIALLY-VANED IMPELLER

The aerodynamic design and experimental performance of a centrifugal compressor designed for a pressure ratio of 6.5 and a specific speed of 68 are described. The compressor consisted of a radially-vaned impeller and a transonic, vaned radial diffuser. At design speed a peak overall total-to-total isentropic efficiency of 0.746 was achieved at the maximum pressure ratio of 5.9, rising to 0.79 at a pressure ratio of 3.5 at 80 per cent speed. A theoretical analysis of the

ARC CP No.1385
September 1976
Jones, M.G.

THE PERFORMANCE OF A 6.5 PRESSURE RATIO CENTRIFUGAL COMPRESSOR HAVING A RADIALLY-VANED IMPELLER

The aerodynamic design and experimental performance of a centrifugal compressor designed for a pressure ratio of 6.5 and a specific speed of 68 are described. The compressor consisted of a radially-vaned impeller and a transonic, vaned radial diffuser. At design speed a peak overall total-to-total isentropic efficiency of 0.746 was achieved at the maximum pressure ratio of 5.9, rising to 0.79 at a pressure ratio of 3.5 at 80 per cent speed. A theoretical analysis of the

ARC CP No.1385
September 1976
Jones, M.G.

THE PERFORMANCE OF A 6.5 PRESSURE RATIO CENTRIFUGAL COMPRESSOR HAVING A RADIALLY-VANED IMPELLER

The aerodynamic design and experimental performance of a centrifugal compressor designed for a pressure ratio of 6.5 and a specific speed of 68 are described. The compressor consisted of a radially-vaned impeller and a transonic, vaned radial diffuser. At design speed a peak overall total-to-total isentropic efficiency of 0.746 was achieved at the maximum pressure ratio of 5.9, rising to 0.79 at a pressure ratio of 3.5 at 80 per cent speed. A theoretical analysis of the

ARC CP No.1385
September 1976
Jones, M.G.

THE PERFORMANCE OF A 6.5 PRESSURE RATIO CENTRIFUGAL COMPRESSOR HAVING A RADIALLY-VANED IMPELLER

The aerodynamic design and experimental performance of a centrifugal compressor designed for a pressure ratio of 6.5 and a specific speed of 68 are described. The compressor consisted of a radially-vaned impeller and a transonic, vaned radial diffuser. At design speed a peak overall total-to-total isentropic efficiency of 0.746 was achieved at the maximum pressure ratio of 5.9, rising to 0.79 at a pressure ratio of 3.5 at 80 per cent speed. A theoretical analysis of the

impeller channel flow suggests that high vane-to-vane aerodynamic loading was partly responsible for the shortfall in performance. The impeller was also tested with a vaneless diffuser and a detailed analysis is made of static pressure measurements on the impeller shroud and vaneless and vaned diffuser walls. Several recommendations are made regarding the design and testing of centrifugal compressors.	impeller channel flow suggests that high vane-to-vane aerodynamic loading was partly responsible for the shortfall in performance. The impeller was also tested with a vaneless diffuser and a detailed analysis is made of static pressure measurements on the impeller shroud and vaneless and vaned diffuser walls. Several recommendations are made regarding the design and testing of centrifugal compressors.
impeller channel flow suggests that high vane-to-vane aerodynamic loading was partly responsible for the shortfall in performance. The impeller was also tested with a vaneless diffuser and a detailed analysis is made of static pressure measurements on the impeller shroud and vaneless and vaned diffuser walls. Several recommendations are made regarding the design and testing of centrifugal compressors.	impeller channel flow suggests that high vane-to-vane aerodynamic loading was partly responsible for the shortfall in performance. The impeller was also tested with a vaneless diffuser and a detailed analysis is made of static pressure measurements on the impeller shroud and vaneless and vaned diffuser walls. Several recommendations are made regarding the design and testing of centrifugal compressors.